Measurements and Analysis of Angular Characteristics and Spatial Correlation for High-Speed Railway Channels

Tao Zhou, *Member, IEEE*, Cheng Tao, *Member, IEEE*, Sana Salous, *Senior Member, IEEE*, and Liu Liu, *Member, IEEE*

***Abstract*— Spatial characteristics of the propagation channel have a vital impact on the application of multi-antenna techniques. This paper analyzes angular characteristics and the spatial correlation for high-speed railway (HSR) channels, based on a novel moving virtual antenna array (MVAA) measurement scheme. The principle of the MVAA scheme is deeply investigated and is further verified by a theoretical geometry-based stochastic model. Using the MVAA scheme, virtual single-input multiple-output (SIMO) channel impulse response data are derived from single-antenna measurements in typical HSR scenarios, involving viaduct, cutting, and station. Based on the SIMO channel data, angle of arrival is extracted according to the unitary estimation of signal parameters by the rotational invariance techniques algorithm, and is compared with the theoretical result. Moreover, power angular spectrum and root mean square (rms) angular spread (AS) are provided, and the rms AS results are statistically modeled and comprehensively compared. In addition, spatial correlation is calculated and analyzed, and a rms AS-dependent spatial correlation model is newly proposed to describe the relationship between the angular dispersion and the spatial correlation. The presented results could be used in multi-antenna channel modeling and will facilitate the assessment of multi-antenna technologies for future HSR mobile communication systems.**

***Index Terms*— High-speed railway channel, virtual antenna array, angualr characteristics, spatial correlation, channel modeling.**

I. Introduction

As WITH the previous generation systems, the upcoming fifth-generation (5G) mobile communication system will cover not only conventional cellular scenarios but also high mobility scenarios, such as highway, subway, and high-speed railway (HSR) [1]. Although 5G aims at delivering a consistent experience across a variety of scenarios, it is a great challenge for 5G solutions to provide a satisfactory service to passengers on high-speed trains at a speed of up to 500 km/h [2]. Thus, the application of 5G techniques in HSR scenarios are attracting more attention.

It is expected that 5G will be able to support 0.1∼1 Gbps user experienced data rate and tens of Gbps peak data rate [3]. AQ:2 In order to meet the requirement of such high data rate, multiple-input multiple-output (MIMO) and massive MIMO [4], which exploit the spatial domain of mobile fading to enhance system capacity, will be the key supporting techniques in 5G. Intuitively, the HSR is not a favorable environment for using multi-antenna techniques, due to the line-of-sight (LOS) dominance [5]. However, there exist a wide variety of propagation scenarios on HSR, such as urban, suburban, rural, hilly, as well as a number of special scenarios like cutting, viaduct, tunnel, station, and so on, some of which could have rich scattering and reflecting components [6]. To apply the multi-antenna techniques on HSR, it is quite necessary to investigate spatial characteristics in various HSR scenarios.

The spatial characteristics of the propagation channel can be classified into two categories: angular characteristics and spatial correlation. The former is an indispensable part in spatial channel modeling, while the latter is a popular parameter to evaluate the performance of multi-antenna techniques. So far, most of the studies have concentrated on the large-scale fading, delay dispersion and frequency dispersion in HSR channels [7]–[11]. However, there are few works referring to the spatial characteristics in the HSR environments. Angular characterization for HSR channel was first presented in [12] where root mean square (RMS) angular spread (AS) was obtained from single-input multiple-output (SIMO) measurements using the relay coverage (RC) scheme. Although the well-known WINNER II model [13] includes the RMS AS result into the D2a scenario which is regarded as a kind of fast train scenario, it does not specify the applicable HSR scenarios, e.g., viaduct, cutting or station. In [14], multi-antenna measurements considering the direct coverage (DC) scheme were conducted for analyzing angle of arrival (AOA) and RMS AS parameters in specific HSR environments, including an agricultural area and a hilly district. However, the angular characteristics derived from the DC measurement

Manuscript received October 17, 2016; revised January 19, 2017 and February 21, 2017; accepted March 2, 2017. This work was supported in part by the National Natural Science Foundation of China under Grant 61371070 and Grant 61471030, in part by the Beijing Natural Science Foundation under Grant 4174102, in part by the Fundamental Research Funds for the Central Universities under Grant 2016RC031, and in part by the Open Research Fund through the National Mobile Communications Research Laboratory, Southeast University, under Grant 2014D05. The Associate Editor for this paper was AQ:1 X. Cheng. *(Corresponding authors: Liu Liu and Cheng Tao.)*

T. Zhou and L. Liu are with the Institute of Broadband Wireless Mobile Communications, Beijing Jiaotong University, Beijing 100044, China (e-mail: zhou@bjtu.edu.cn; liuliu@bjtu.edu.cn).

C. Tao is with the Institute of Broadband Wireless Mobile Communications, Beijing Jiaotong University, Beijing 100044, China, and also with the National Mobile Communications Research Laboratory, Southeast University, Nanjing 210096, China (e-mail: chtao@bjtu.edu.cn).

S. Salous is with the School of Engineering and Computing Sciences, Durham University, Durham DH1 3LE, U.K. (e-mail: sana.salous@durham.ac.uk).

Color versions of one or more of the figures in this paper are available online at http://ieeexplore.ieee.org.

Digital Object Identifier 10.1109/TITS.2017.2681112

embody the effect of scatterers and reflectors inside the train carriage, which cannot represent the realistic angular dispersion in the outdoor propagation environment of HSR. Based on a 2×2 MIMO RC measurement in HSR viaduct scenarios, [15] initially discussed the spatial correlation of the HSR channel, which shows that the correlation coefficient varies from a higher value to a lower value as the train moves far away from base station (BS). In addition, some theoretical channel models, such as geometry-based stochastic model (GBSM) [16]–[18] and propagation graph-based model [19], [20], have been used to analyze the spatial characteristics in numerous HSR environments. Although the theory-based models are convenient for the analysis and simulation of the multi-antenna channel, they still need the support of actual measurement data.

It is well-known that performing multi-antenna channel measurements on HSR is highly difficult because of some measurement constraints [21]. The lack of multi-antenna measurement data leads to a huge gap of the spatial characteristics on HSR multi-antenna channel modeling and performance evaluation. To overcome the difficulty of the HSR multi-antenna channel measurements, a moving virtual antenna array (MVAA) measurement scheme has been proposed and verified in [22], which employs a single antenna to simulate multiple virtual antennas. A similar scheme was applied in MIMO and massive MIMO measurements for indoor static scenarios [23], [24]. According to the MVAA scheme, AOA estimation was implemented based on single-antenna measurements in HSR viaduct scenarios [25]. However, the specific HSR spatial characteristics are not given.

To fill the aforementioned research gaps, this paper provides detailed analysis of angular characteristics and spatial correlation in typical HSR scenarios, involving viaduct, cutting, and station. The major contributions and novelties of this paper are as follows.

1) The MVAA scheme is deeply investigated and is further verified by a GBSM from the theoretical perspective. According to single-antenna measurements and the validated MVAA scheme, virtual SIMO channel data in the three HSR scenarios are generated for spatial characterization.

2) The AOA and power angular spectrum (PAS) are extracted depending on the virtual SIMO channel data. The RMS AS is obtained and statistically modeled, and compared in various HSR scenarios. The acquired RMS AS results will be useful for HSR multi-antenna channel modeling.

3) The spatial correlation in the three HSR environments is analyzed, and the RMS AS-dependent spatial correlation model is proposed to describe the relationship between the angular dispersion and the spatial correlation, which will facilitate HSR multi-antenna technique evaluation.

The remainder of this paper is outlined as follows. Section II highlights the MVAA measurement scheme. In Section III, the virtual SIMO measurement data are acquired. Angular characteristics and spatial correlation are presented in Section IV and Section V, respectively. Finally, conclusions are drawn in Section VI.

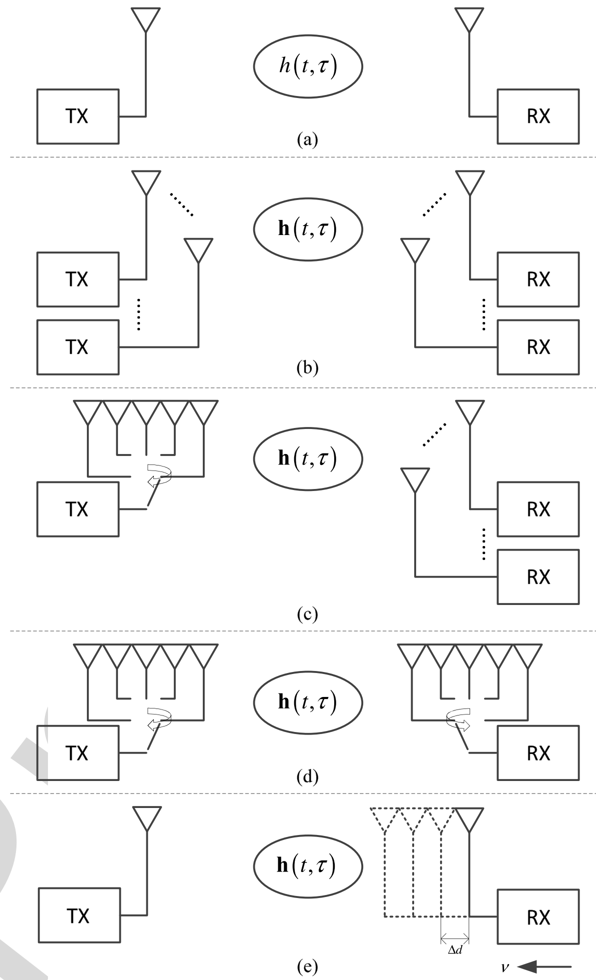

Fig. 1. Channel sounding schemes. (a) SISO scheme. (b) Full parallel scheme. (c) Semi-sequential scheme. (d) Fully sequential scheme. (e) MVAA scheme.

II. Moving Virtual Antenna Array Measurement Scheme

A. Principle

In radio channel sounding, a known signal that repeats at a rate twice the highest expected Doppler shift is transmitted, and the received signal is analyzed to extract the channel impulse response (CIR). The SISO channel sounding scheme that employs a single transmitter (TX) and a single receiver (RX) is most commonly used, as displayed in Fig. 1(a). For conventional multi-antenna channel sounding schemes, they can be classified into three categories [26], as shown in Fig. 1(b)-(d): 1) Full parallel scheme at both the TX and at the RX using a number of orthogonal techniques such as code division multiplexing (CDM) and frequency division multiplexing (FDM); 2) Semi-sequential scheme with time division multiplexing (TDM) at the TX only with parallel receive channels; 3) Fully sequential scheme with TDM at both ends of the link. The full parallel scheme is capable of measuring time-variant channels without restriction. However, for TDM schemes, due to the sequential nature of the measurement, the time required to complete a single sequential measurement depends on the size of the arrays and the repetition time of the sounding waveform. Such sequential measurements should ensure that the channel is either stationary or quasi-stationary during the time of the measurement.

According to the idea of the sequential measurement, a novel MVAA scheme with the advantages of low-cost and low-complexity is proposed, as shown in Fig. 1(e). The proposed scheme employs the hardware that is the same as applied in the SISO scheme. In addition, it does not require fast switches that have to be used in the semi-sequential or fully sequential scheme to control the antenna arrays. When the TX is static and the RX is moving toward the TX with a stable speed, the neighboring samples of the measured CIR can be regarded as several virtual antenna elements. These virtual antenna elements are distributed equally and form a uniform linear array (ULA) with the direction parallel to the moving track. In order to generate the ULA, two important parameters, the element spacing and the element number, should be known.

The element spacing of the ULA is related to the moving speed υ and the repetition time of the sounding waveform T_{rep}, expressed as

$$\Delta d = \upsilon T_{rep}. \tag{1}$$

In general, there are two solutions used to determine Δd, including speed-sensor solution and GPS solution. Here, the speed-sensor solution is recommended because of the higher precision.

On the other hand, the element number of the ULA in the MVAA scheme should be limited. To enable the MVAA scheme, the basic criterion is that the channel should be constant in the duration of the samples which are used to generate the ULA. Thus, the duration that refers to the element number of the ULA M and T_{rep} should be no more than the channel coherence time T_c, expressed as

$$(M-1)\cdot T_{rep} \leq T_c. \tag{2}$$

In Equation (2), the coherence time is used to quantify the element number. In fact, stationarity distance (SD) which has been presented in [27] for the V2V channel and [28] for the air-ground channel is more appropriate than the coherence time. The SD is the duration over which the channel can be assumed stationarity, and it includes not only Doppler shift, but also LOS condition, multipath and more channel effects. However, it is known that the SD for the HSR channel is still unknown. Thus, this paper only simply consider the coherence time.

Assuming that $T_c = 1/B_d$ [29], where $B_d = 2f_{\max}$ is the Doppler spread, $f_{\max} = \upsilon/\lambda$ is the highest Doppler shift, and λ is the wavelength, Equation (2) is rewritten as

$$M \leq 1 + \frac{1}{2\cdot f_{\max} T_{rep}} = 1 + \frac{\lambda/2}{\Delta d}. \tag{3}$$

From Equation (3), M is inversely proportional to Δd, which means that the smaller the duration of the samples is, the more virtual antenna elements can be included in the ULA. In addition, the maximum Δd cannot exceed $\lambda/2$ so that a minimum two-element ULA can be established. If $\Delta d > \lambda/2$, $M = 1$ and the MVAA scheme would be invalid. On the other hand, $\Delta d > \lambda/2$ would lead to a set of cyclically ambiguous AOA estimates, in accordance with the spatial Nyquist sampling theorem [30]. Thus, to achieve the MVAA scheme, $\Delta d \leq \lambda/2$ should be satisfied.

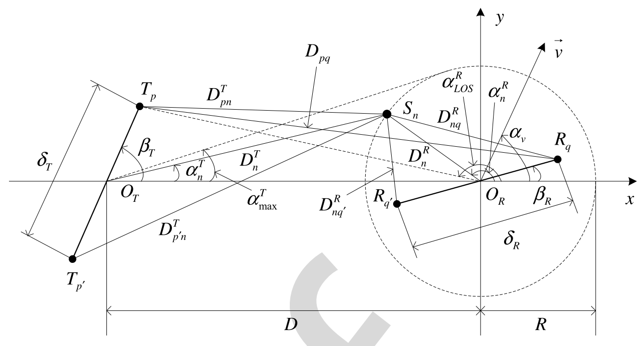

Fig. 2. A 2×2 GBSM with one-ring architecture.

B. Validation

In order to validate the MVAA scheme, a 2×2 GBSM with the classical one-ring architecture is considered, as shown in Fig. 2 [31]. The RX is surrounded by local scatterers S_n, $n = 1, 2, \ldots, N$. The TX and RX antenna element spacings are denoted by δ_T and δ_R, and the tilt angles of the arrays are represented by β_T and β_R, respectively. The ring radius is R and the distance between TX and RX is D. The angle-of-motion α_υ indicates the angle between the x-axis and the direction of motion with the speed of υ. The symbol $\alpha^T_{\max}$ stands for the maximum AOD seen from the TX. This quantity is related to R and D by $\alpha^T_{\max} = \arctan(R/D) \approx R/D$. Moreover, it is assumed that both R and D are large compared to the geometrical size of the antenna arrays, i.e., $D \gg R \gg \max\{\delta_T, \delta_R\}$.

According to the established GBSM, the closed-form expression of space-time (ST) correlation function (CF) between two subchannels $h_{pq}(t)$ and $h_{p'q'}(t)$ can be derived by [32], [33]

$$\rho_{h_{pq},h_{p'q'}}(\delta_T, \delta_R, \tau) = \frac{E\left[h_{pq}(t)\, h^*_{p'q'}(t+\tau)\right]}{\sqrt{\Omega_{pq}\Omega_{p'q'}}}, \tag{4}$$

where Ω_{pq} and $\Omega_{p'q'}$ denote the total power of the T_p-R_q link and $T_{p'}$-$R_{q'}$ link, and $(\cdot)^*$ indicates the complex conjugate.

In case of isotropic scattering, substituting $\delta_T = \delta_R = 0$ and $\tau = 0$ into the closed-form expression of ST CF, the time CF and the space CF can be respectively obtained as [34]

$$\rho_{h_{pq},h_{p'q'}}(0,0,\tau) = J_0(2\pi f_{\max}\tau), \tag{5}$$

and

$$\begin{aligned}
&\rho_{h_{pq},h_{p'q'}}(\delta_T, \delta_R, 0) \\
&\quad = e^{j2\pi\frac{\delta_T}{\lambda}\cos(\beta_T)} J_0(2\pi\{(\frac{\delta_R}{\lambda})^2 \\
&\qquad + (\frac{\delta_T}{\lambda}\alpha^T_{\max}\sin\beta_T)^2 \\
&\qquad + 2\frac{\delta_T\delta_R}{\lambda^2}\alpha^T_{\max}\sin\beta_T\sin\beta_R\}^{1/2}),
\end{aligned} \tag{6}$$

where $J_0(\cdot)$ denotes the zeroth-order Bessels function of the first kind.

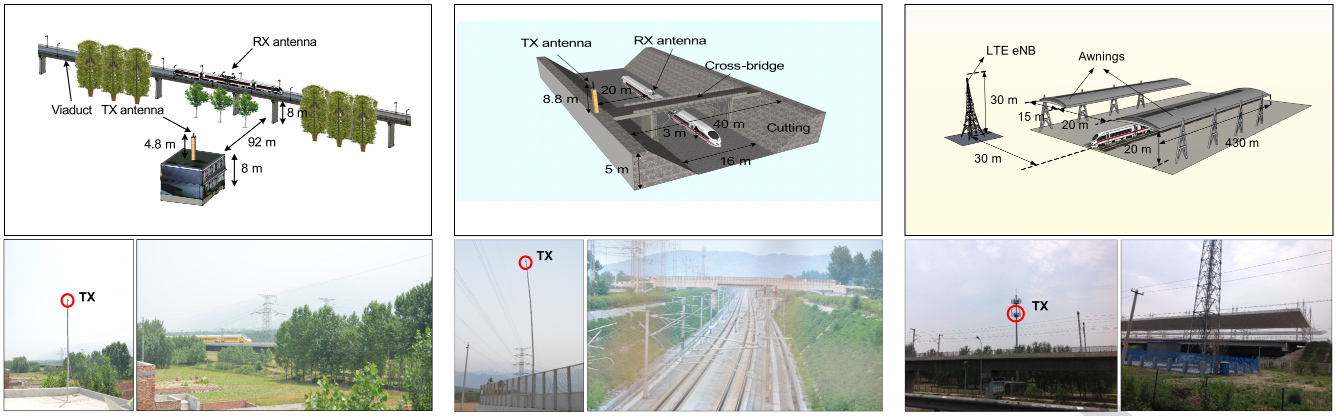

(a) (b) (c)

Fig. 3. Overview of the measured scenarios. (a) Viaduct. (b) Cutting. (c) Station.

TABLE I
MEASUREMENT CONFIGURATION

Scenario	Viaduct	Cutting	Station
Equipment	Propsound	Propsound	LTE Sounder
Carrier frequency	2350 MHz	2350 MHz	1890 MHz
TX power	30.8 dBm	32.7 dBm	CRS: 12.2 dBm
Bandwidth	50 MHz	50 MHz	18 MHz
Waveform repetition frequency	1968.5 Hz	1968.5 Hz	2000 Hz
TX antenna height	12.8 m	13.8 m	30 m
RX antenna height	11 m	3 m	10 m
Distance between TX and railway track	92 m	30 m	30 m
Train velocity	198 km/h	198 km/h	285 km/h

Applying the MVAA scheme to the GBSM model, i.e., setting $\delta_T = 0$ and $\delta_R = \Delta d$, the space CF is transformed into

$$\rho_{h_{pq},h_{p'q'}}(0, \Delta d, 0) = J_0\left(2\pi v T_{rep}/\lambda\right) = \rho_{h_{pq},h_{p'q'}}(0, 0, \tau). \quad (7)$$

Equation (7) shows that according to the MVAA scheme, the space CF in the GBSM model equals the time CF. This confirms that the temporal correlation can be equivalent to the spatial correlation by using the MVAA scheme. Thus, it is possible to employ the single-antenna measurement data to perform the analysis of spatial characteristics. In the next section, the virtual multi-antenna measurement data will be generated based on realistic single-antenna measurements and the validated MVAA scheme.

III. VIRTUAL SIMO MEASUREMENT DATA

A. Measurement Campaigns

Both positive and passive sounding approaches [35] are employed in the single-antenna channel measurements for three typical HSR scenarios. Propsound, a positive channel sounder, is used to conduct RC channel measurements in viaduct and cutting scenarios on Zhengzhou to Xi'an HSR in China [36]. The TX equipped with a vertical-polarized dipole antenna is placed near the railway track to send out an excitation signal. The RX is positioned inside the train carriage and employs a special train-mounted antenna, HUBER+SUHNER [37], to collect the test signal. In addition, a passive long-term evolution (LTE) sounder is employed to perform RC measurements in a station scenario on Beijing to Tianjin HSR in China [38]. The LTE eNodeB (eNB) in the specialized railway network transmits LTE signal by a directional antenna. The LTE sounder utilizes the HUBER+SUHNER antenna to collect the LTE signal and extracts CIR from cell-specific reference signal (CRS). The specific measurement configuration for the three scenarios is listed in Table I. The measured scenarios are shown in Fig. 3, which have some special features as follows.

1) Viaduct: There are some obvious local scatterers around the viaduct, such as dense trees which are much higher than the train-mounted antenna. These local scatterers will hinder the propagation of radio waves and result in serious channel dispersion. The height of TX antenna is not dominant compared to the RX antenna due to the limited test condition. In this case, the effect of shadowing will be further intensified.

2) Cutting: There are few obstacles in the cutting that seems a semi-closed structure with steep walls on both sides of the railway track. However, since the slopes are usually covered by vegetation, they will produce a great deal of extra reflections and scattering. Moreover, the RX is lower than the steep walls leading to a deep cutting scenario which leads to more multipath components [39]. Especially, there exists a cross-bridge used for setting the TX antenna, which could result in short term blockage of the propagation path.

3) Station: The train with 200-m length, 4-m height, and 3-m width is running through the station under a viaduct with 10-m height. The measured station can be regarded as an open-type station in which the awnings only cover the platform

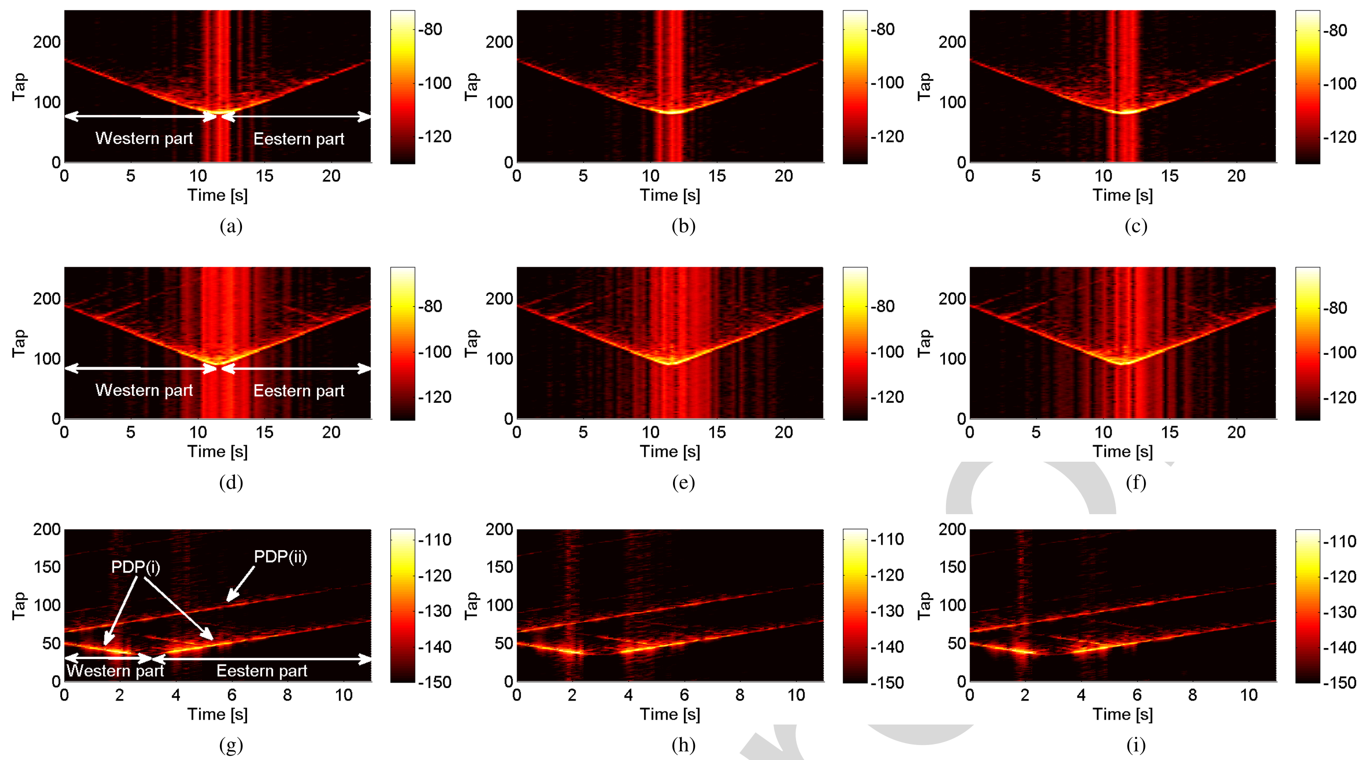

Fig. 4. Time-variant PDPs for h_1, h_2, h_3 in different scenarios. (a-c) Viaduct. (d-f) Cutting. (g-i) Station.

supporting a clear free space over the rail [40]. However, the awnings can still produce lots of scattering and reflections to complicate the fading behavior.

B. Data Processing

The CIR is continuously captured by Propsound and the LTE sounder at a certain interval. This interval is inversely proportional to the waveform repetition frequency (WRF) that should be at least twice the maximum expected Doppler shift. In the viaduct and cutting scenarios, the used CIR data contain 45108 snapshots with a time interval of 0.51-ms, corresponding to 22.9-s duration. In the station environment, the analyzed CIR data consist of 22010 snapshots with a time interval of 0.5-ms, corresponding to 11-s duration. Each snapshot comprises the multipath taps of 254 for the Propsound measurement and 200 for the LTE sounder measurement.

Substituting the values listed in Table I into Equation (3), $M < 3.28$ for the viaduct and cutting scenarios and $M < 3.01$ for the station scenario, which indicates that the virtual array can support a maximum of three elements. Here, the speed-sensor solution is considered and the stable train speed is assumed. Then the three-element virtual ULA with the spacing of 0.22λ and 0.25λ for Propsound and LTE sounder measurements is respectively generated. The CIR from the TX to the m-th virtual receive element ($m = 1, 2, 3$) is derived by

$$h_m(t, \tau) = h(t_{3k+m}, \tau), \quad k = 0, 1, 2... \tag{8}$$

Finally, the multiple-antenna channel data $\mathbf{h}(t, \tau) = [h_1(t, \tau)\ \ h_2(t, \tau)\ \ h_3(t, \tau)]$ are obtained, which can be used for the spatial characterization.

Fig. 4 illustrates the time-variant power delay profiles (PDPs) for h_1, h_2, h_3 in the measured three HSR scenarios. The unit in the colorbars of Fig. 4 is dB. In the viaduct and cutting scenarios, the strongest LOS component is observed when the RX is closest to the TX at around 11.5-s and its power becomes weaker as the RX moves far away from the TX. The whole measurement data can be divided into two parts, the western part and the eastern part. As for the station scenario, two obvious PDP transitions, PDP(i) and PDP(ii), are found in the measurement. The PDP(i) belongs to the propagation channel from the primary eNB to the sounder, whereas the CIR(ii) is caused by the neighboring eNB. The PDP(i) and PDP(ii) can be distinguished in the delay domain according to the method mentioned in [38]. Here, only PDP(i) is used to extract the spatial characteristics. Regarding the PDP(i), the power of the multipath components is weaker when the RX is closest to the TX at around 3-s. This is because the train is underneath the eNB antenna, and the RX is not in the mainlobe of the antenna pattern of the directional antenna [41]. Similar to the viaduct and cutting scenarios, the PDP(i) data in the station measurement can be also classified into the western part and the eastern part.

IV. Results and Discussions

A. Angle of Arrival Estimation

The estimation of signal parameters by the rotational invariance techniques (ESPRIT) algorithm which creates the signal subspace and then extracts the angle information in closed form is capable of analyzing the AOA in azimuth at the RX side. Comparing various ESPRIT algorithms, Unitary ESPRIT [42], [43] is employed due to the lower complexity

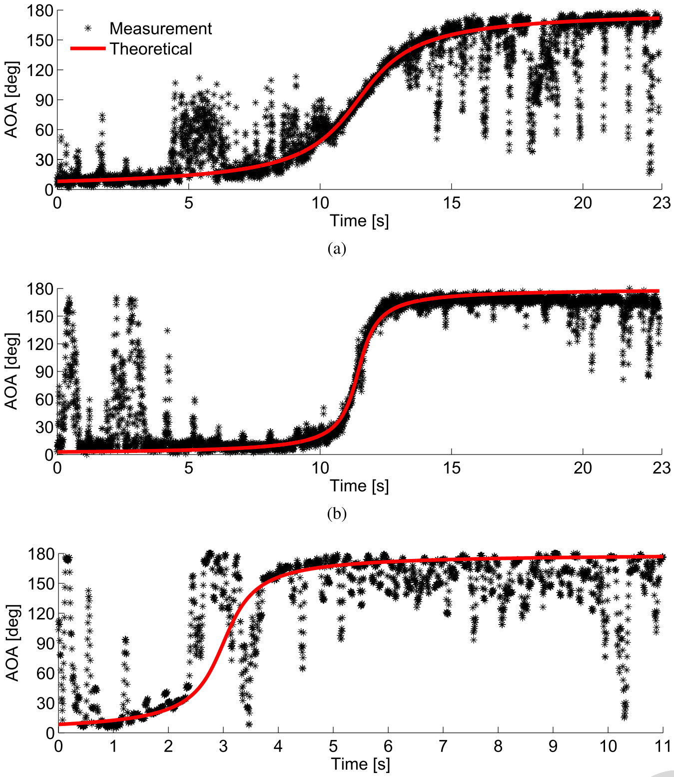

Fig. 5. Time-variant AOAs in different scenarios. (a) Viaduct. (b) Cutting. (c) Station.

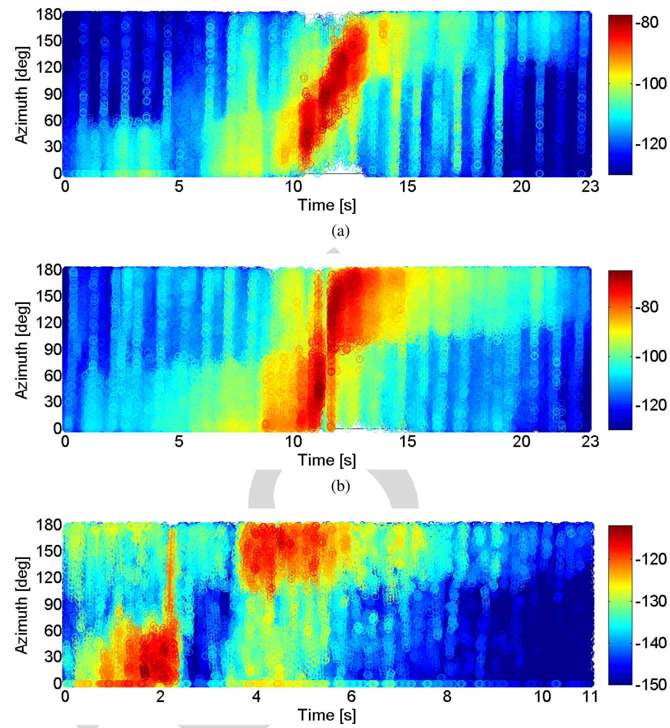

Fig. 6. Instantaneous PASs in different scenarios. (a) Viaduct. (b) Cutting. (c) Station.

and higher accuracy. For the usage of the common Unitary ESPRIT, there are two restrictions: 1) the antenna array should be ULA, otherwise 2-D Unitary ESPRIT algorithms are required [44]; 2) the number of incident waves whose direction can be estimated should be less than the amount of antenna array elements. Since the three-element ULA is generated in the virtual SIMO measurements, the simple 1-D Unitary ESPRIT can be used. However, due to the limited element number of the MVAA, only one or two incident waves for each cluster can be identified. Such low resolution leads to the difficulty of analyzing the cluster-wise angle information. Thus, this paper mainly concentrates on the global angle parameters which are also of interest in the geometric MIMO channel modeling [14].

The Unitary ESPRIT algorithm is applied to the virtual SIMO measurement data $h(t, \tau_l)$ and provides the estimate of AOA associated with the l-th delay. Fig. 5 shows the AOA results for the strongest cluster in the three scenarios. The theoretical AOA for the LOS condition, as a reference, is also shown in Fig. 5. In [45], the theoretical time-varying AOA is given as

$$\hat{\theta}(t) = \arccos\left\{\frac{v(t_0 - t)}{\sqrt{d_{\min}^2 + [v(t - t_0)]^2}}\right\}, \quad 0 \le t \le t_0, \tag{9}$$

where $d_{\min}$ denotes the minimum distance between TX and RX, i.e., the distance between the train and the railway track. t_0 represents the moment when the TX passes by the RX, i.e., when the distance between TX and RX equals $d_{\min}$.

It is observed from Fig. 5 that there is a good match between the measured and theoretical results with regard to the overall AOA variation. The AOA changes approximately from 0° to 180° due to the impact of the movement of the train. Since the TX in the cutting or station scenarios is much closer to the railway track, the variation in the cutting or station scenarios is faster than that in the viaduct scenario when the train passes through the TX. It is also found that the AOA values in some regions have a larger deviation from the theoretical results. This is because there are non-LOS (NLOS) clusters appearing in the regions, such as the coverage areas of the dense trees in the viaduct scenario, the cross-bridge in the cutting scenario, and the awnings in the station scenario. Furthermore, it is seen that there is a dramatic fluctuation around 3-s in the station scenario since the train is located in the sidelobe of the directional antenna.

B. Power Angular Spectrum

Using the estimated AOAs, an array steering matrix can be formed. For the ULA, the array steering matrix can be constructed as

$$\mathrm{A}_\Theta = \begin{bmatrix} 1 & 1 & \cdots & 1 \\ e^{j\frac{2\pi\Delta d\sin\theta_1}{\lambda}} & e^{j\frac{2\pi\Delta d\sin\theta_2}{\lambda}} & \cdots & e^{j\frac{2\pi\Delta d\sin\theta_P}{\lambda}} \\ \vdots & \vdots & \ddots & \vdots \\ e^{j\frac{2\pi(M-1)\Delta d\sin\theta_1}{\lambda}} & e^{j\frac{2\pi(M-1)\Delta d\sin\theta_2}{\lambda}} & \cdots & e^{j\frac{2\pi(M-1)\Delta d\sin\theta_P}{\lambda}} \end{bmatrix}, \tag{10}$$

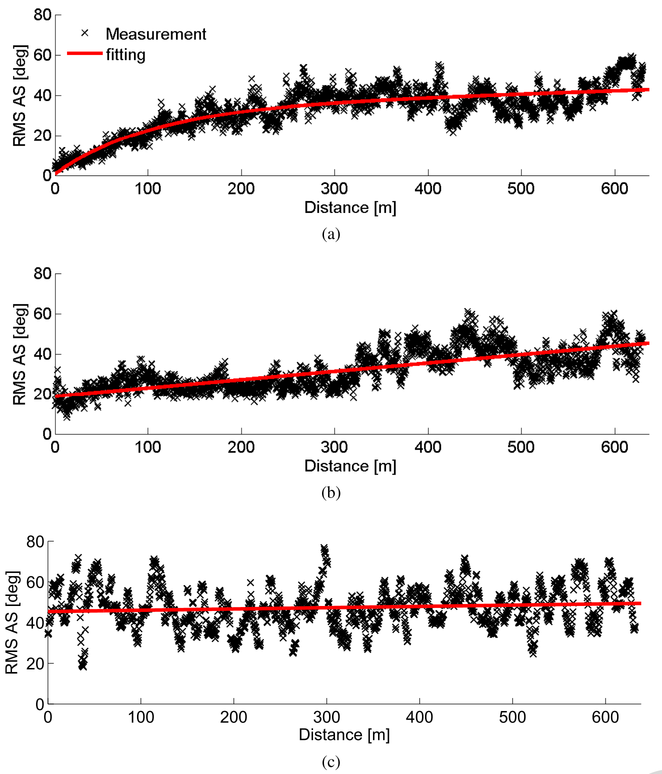

Fig. 7. Distance-dependent RMS AS in different scenarios. (a) Viaduct. (b) Cutting. (c) Station.

where P is the number of identifiable incident waves, P should be smaller than M, and $\Theta = \{\theta_1, \theta_2, \cdots, \theta_P\}$ is the set of the estimated AOAs. Subsequently, the Moore-Penrose pseudoinverse of A_Θ (denoted as $\mathrm{A}_\Theta^\dagger = \left(\mathrm{A}_\Theta^H \mathrm{A}_\Theta\right)^{-1} \mathrm{A}_\Theta^H$) is used to obtain the estimates of incident waves corresponding to the set of AOAs as [46]

$$\begin{aligned} h_\Theta(t, \tau_l) &= \mathrm{A}_\Theta^\dagger h_m(t, \tau_l) \\ &= \left\{h_{\theta_1}(t, \tau_l), h_{\theta_2}(t, \tau_l), \ldots, h_{\theta_P}(t, \tau_l)\right\}. \end{aligned} \tag{11}$$

Based on the extracted AOAs and the corresponding power, the PAS that characterizes how much power arrives on average from a certain angle can be obtained as [47]

$$P_A(t, \theta) = E\left\{\left|\int\int h(t, \tau, \theta)\, d\theta d\tau\right|^2\right\}. \tag{12}$$

Fig. 6 illustrates the instantaneous PAS results in the three scenarios. The unit in the colorbars of Fig. 6 is dB. It is found that the PAS shows a certain spread in all three scenarios. This is due to the presence of the reflectors and scatterers in the measured scenarios, such as dense trees, steep walls, and awnings. These reflectors and scatterers would produce a number of multipath components with different AOAs, thus leading to angular dispersion. In order to specifically characterize the angular dispersion, RMS DS will be extracted and analyzed in the following subsection.

TABLE II
PARAMETERS OF THE RMS AS MODEL

Scenario	Viaduct	Cutting	Station
x_1	34.19	18.78	45.43
y_1	0.00035	0.041	0.0063
x_2	-33.65	-	-
y_2	-0.0095	-	-
σ_θ	5.78	6.63	10.1

C. Angular Spread

The RMS AS is calculated as the root second central moment of the PAS

$$\Delta\theta(t) = \sqrt{\frac{\int \left[\theta(t) - \bar{\theta}(t)\right]^2 P_A(t, \theta)\, d\theta}{\int P_A(t, \theta)\, d\theta}}, \tag{13}$$

where $\bar{\theta}(t)$ is the averaged AOA, expressed as

$$\bar{\theta}(t) = \frac{\int \theta(t) P_A(t, \theta)\, d\theta}{\int P_A(t, \theta)\, d\theta}. \tag{14}$$

The relationship between the channel parameters and the distance is always of interest in channel characterization [47]. Here, $\Delta\theta(t)$ is transformed into the value as a function of the distance $\Delta\theta(d)$, where d denotes the relative horizontal distance between the TX and the RX. Fig. 7 shows the distance-dependent RMS AS results in the three scenarios. It is worth noting that the results in the viaduct and cutting scenarios are the averaged values derived from both the western half and the eastern half of CIR data, whereas the result in the station scenario is only obtained by the eastern half of CIR(i) data. It can be seen that the RMS AS experiences a gradual growth with the distance in the viaduct and cutting scenarios, which means that more clusters that cause the larger AS can be identified as the distance increases. However, the RMS AS remains almost stable in the station scenario. This is because the train is always within the station where the scattering and reflecting conditions are stationary.

To describe the variation of RMS AS, a double exponential function and two linear functions are employed to fit the RMS AS curves using the least square (LS) method in the viaduct, cutting, and station scenarios, respectively, expressed as

$$\Delta\theta'(d) = \begin{cases} x_1 e^{y_1 d} + x_2 e^{y_2 d}, & \text{viaduct} \\ x_1 + y_1 d, & \text{cutting/station.} \end{cases} \tag{15}$$

Then, a distance-dependent statistical model for the RMS AS results is proposed as

$$\Delta\theta(d) = \Delta\theta'(d) + x\sigma_\theta, \tag{16}$$

where $\Delta\theta'(d)$ denotes the mean value of the RMS AS model, x_1, y_1, x_2 and y_2 are the coefficients of the model, σ_θ indicates the standard deviation of the model, and x represents zero-mean Gaussian variable with the unit standard deviation. The model parameters are listed in Table II.

Fig. 8 depicts the cumulative distribution function (CDF) measurement and Normal fitting results of RMS AS in the three scenarios. A detailed comparison of the statistical RMS AS results in the RC and DC schemes for the viaduct, cutting,

TABLE III
COMPARISON OF THE STATISTIC RMS AS RESULTS IN DIFFERENT HSR SCENARIOS

Scenario	Viaduct	Cutting	Station	D2a [13]	Agricultural Area [14]	Hilly District [14]
Coverage scheme	RC	RC	RC	RC	DC	DC
10% of CDF	15.2°	20.8°	34.5°	21.3°	-	-
50% of CDF	34.7°	29.9°	47.8°	30.4°	-	-
90% of CDF	45.6°	46.3°	60.5°	45.9°	-	-
Mean value	32.7°	31.9°	47.4°	32.5°	75°	60°
Standard deviation	12.9°	10.1°	10.2°	-	-	-

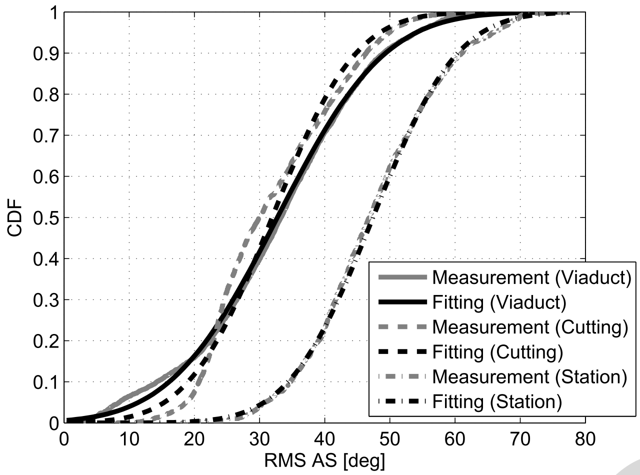

Fig. 8. CDFs of RMS AS in viaduct, cutting and station scenarios.

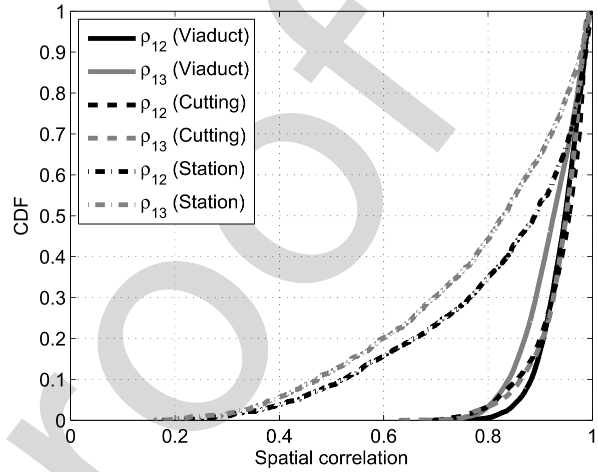

Fig. 9. CDFs of spatial correlation in viaduct, cutting and station scenarios.

station, D2a, agricultural area and hilly district scenarios is shown in Table III. It is observed that the mean value of RMS AS measured in the RC scheme is much smaller than the result obtained in the DC scheme. This confirms that the indoor environment of the train causes additional scattering and reflecting waves, leading to the larger AS. For the RC scheme, it is found that the RMS AS value in the station scenario is much higher than the results in the viaduct, cutting, and D2a scenarios. This is because the station causes more multipath components than the other scenarios. In addition, although 10% and 50% values of RMS AS in the viaduct scenario are respectively lower and higher than those in the cutting scenario, there are similar mean values and 90% values. This means that the measured viaduct scenario with the coverage of dense trees could have the equivalent propagation effect to the cutting scenario as a whole.

D. Spatial Correlation

Spatial correlation between different antenna elements at both ends of the individual link is a key parameter of performance evaluation in MIMO channels. In order to extract the spatial correlation, the wideband data are transformed into the narrowband data $\mathbf{h}(t)$ by making the complex sum of $\mathbf{h}(t, \tau)$ over the delay domain. Then, applying Equation (4) to $\mathbf{h}(t)$, ρ_{12} and ρ_{13} that represent the correlation between $h_1(t)$ and $h_2(t)$ and the correlation between $h_1(t)$ and $h_3(t)$ can be obtained respectively.

Fig. 9 depicts CDF results of ρ_{12} and ρ_{13} with the spacing of $\Delta d_{12} = 0.22\lambda$ and $\Delta d_{13} = 0.44\lambda$ in the viaduct and cutting scenarios and with the spacing of $\Delta d_{12} = 0.25\lambda$ and $\Delta d_{13} = 0.5\lambda$ in the station scenario. It is observed that the spatial correlation in the station scenario is apparently lower than those in the viaduct and cutting scenarios. This confirms that the scattering and reflecting components in the station scenario are much richer. It can be also seen that the correlation decreases as the antenna spacing increases in the three scenarios. Furthermore, 35%∼45% values of correlation are lower than 0.8 in the station scenario when $\Delta d \leq 0.5\lambda$, whereas up to 95% values are higher than 0.8 in the viaduct and cutting scenarios. Thus, it is suggested that in case of $\Delta d \leq 0.5\lambda$, the multi-antenna techniques can be used in the station scenario while it is not suitable in the viaduct and cutting scenarios.

TABLE IV
PARAMETERS OF THE SPATIAL CORRELATION MODEL

Scenario	Viaduct	Cutting	Station
a	-2.73e-5	-2.01e-5	-
b	-0.00053	-0.0016	-0.0045
c	0.99	1.01	1.01
σ_ρ	0.036	0.039	0.18

In most of the reported work, the spatial correlation and the RMS AS are always separately considered. In fact, there is a close relation between the spatial correlation and the RMS AS, as illustrated in Fig. 10. It is noted that the spatial correlation decreases with the increase of the RMS AS in the three scenarios. In order to quantitatively describe the relation of the two parameters, a RMS AS-based spatial correlation

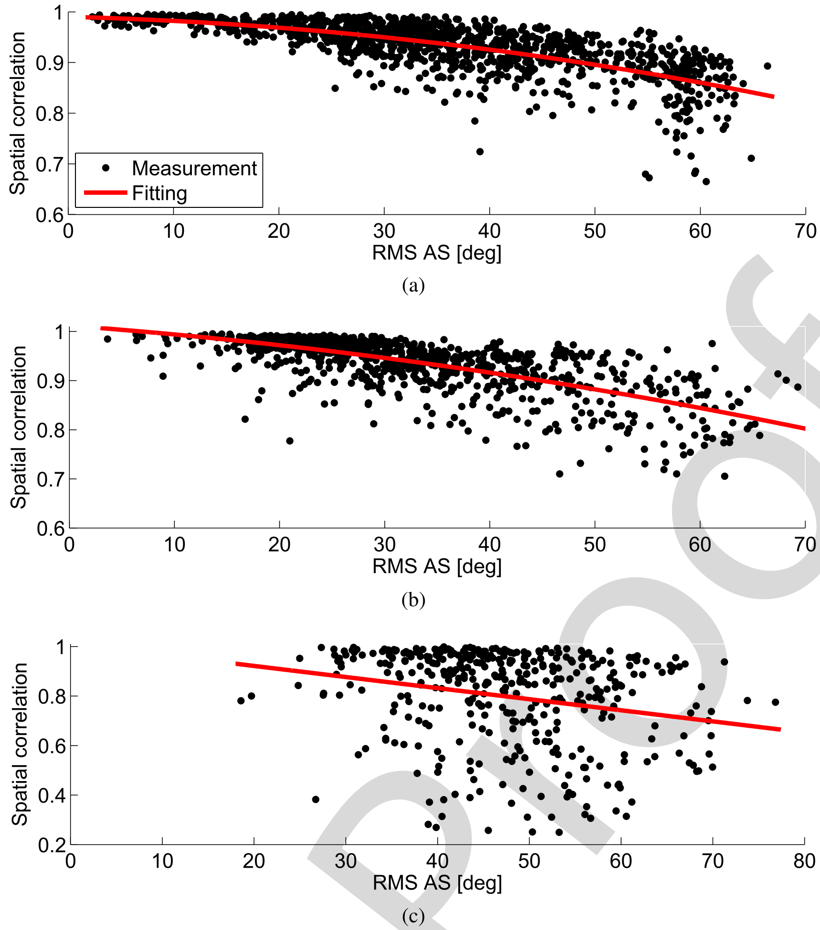

Fig. 10. RMS AS-dependent spatial correlation in different scenarios. (a) Viaduct. (b) Cutting. (c) Station.

model is established as

$$\rho(\Delta\theta) = \begin{cases} a\Delta\theta^2 + b\Delta\theta + c + y\sigma_\rho, & \text{viaduct/cutting} \\ b\Delta\theta + c + y\sigma_\rho, & \text{station,} \end{cases} \quad (17)$$

where, a, b, and c denote the model parameters, σ_ρ indicates the standard deviation of the model, and y represents zero-mean Gaussian variable with the unit standard deviation. The model coefficients are listed in Table IV. Using the proposed spatial correlation model, it could be convenient to determine the spatial correlation coefficient based on the RMS AS value, and then it is possible to evaluate the MIMO performance depending on the RMS AS results.

V. Conclusion

This paper presents the analysis of the angular characteristics and spatial correlation in the HSR viaduct, cutting and station scenarios. The multi-antenna CIR data obtained according to the validated MVAA scheme and the SISO measurements are used for the spatial characterization. It is shown that the AOA estimated by the Unitary ESPRIT algorithm has a reasonable consistency with the theoretical result, and the derived PAS confirms the angular dispersion in the HSR channel. The angular dispersion is statistically characterized by the distance-based RMS AS model, and the statistical RMS AS results are compared in various HSR scenarios. It is also shown that when the antenna spacing is around 0.5 wavelength, almost all spatial correlation values are higher than 0.8 in the viaduct and cutting environments, however up to 45% of the values are lower than 0.8 in the station environment. Additionally, the proposed RMS AS-dependent spatial correlation model is able to efficiently describe the relationship between the angular dispersion and the spatial correlation. These results will provide useful information for channel modeling and performance evaluation in HSR multi-antenna communication systems.

References

[1] X. Cheng, L. Yang, and X. Shen, “D2D for intelligent transportation systems: A feasibility study,” *IEEE Trans. Intell. Transp. Syst.*, vol. 16, no. 4, pp. 1784–1793, Aug. 2015.

[2] *White Paper for 5G High Mobility*. [Online]. Available: http://www.future-forum.org/ AQ:3

[3] *White Paper on 5G Vision and Requirements*. [Online]. Available: http://www.imt-2020.cn/

[4] T. L. Marzetta, “Noncooperative cellular wireless with unlimited numbers of base station antennas,” *IEEE Trans. Wireless Commun.*, vol. 9, no. 11, pp. 3590–3600, Nov. 2010.

[5] T. Zhou, C. Tao, L. Liu, J. Qiu, and R. Sun, “High-speed railway channel measurements and characterizations: A review,” *J. Modern Transp.*, vol. 20, no. 4, pp. 199–205, Dec. 2012.

[6] B. Ai *et al.*, “Radio wave propagation scene partitioning for high-speed rails,” *Int. J. Antennas Propag.*, vol. 2012, pp. 815232-1–815232-7, Dec. 2012. AQ:4

[7] B. Ai *et al.*, “Challenges toward wireless communications for high-speed railway,” *IEEE Trans. Intell. Transp. Syst.*, vol. 15, no. 5, pp. 2143–2158, Oct. 2014.

[8] C.-X. Wang, A. Ghazal, B. Ai, Y. Liu, and P. Fan, "Channel measurements and models for high-speed train communication systems: A survey," *IEEE Commun. Surveys Tut.*, vol. 18, no. 2, pp. 974–987, 2nd Quart., 2016.

[9] R. He, B. Ai, Z. Zhong, A. F. Molisch, R. Chen, and Y. Yang, "A measurement-based stochastic model for high-speed railway channels," *IEEE Trans. Intell. Transp. Syst.*, vol. 16, no. 3, pp. 1120–1135, Jul. 2014.

[10] K. Guan *et al.*, "Excess propagation loss modeling of semiclosed obstacles for intelligent transportation system," *IEEE Trans. Intell. Transp. Syst.*, vol. 17, no. 8, pp. 2171–2181, Aug. 2016.

[11] L. Liu *et al.*, "Position-based modeling for wireless channel on high-speed railway under a viaduct at 2.35 GHz," *IEEE J. Sel. Areas Commun.*, vol. 30, no. 4, pp. 834–845, May 2012.

[12] MEDAV. (2008). *RUSK Measurement Campaigns Overview*. [Online]. Available: http://www.medav.de/

[13] P. Kyösti *et al.*, "WINNER II channel models part II radio channel measurement and analysis results," 2007. AQ:5

[14] R. Parviainen, P. Kyösti, and Y. Hsieh, "Results of high speed train channel measurements," Eur. Cooperat. Field Sci. Tech. Res., Tech. Rep., 2008. AQ:6

[15] Q. Wang, C. Xu, M. Zhao, and D. Yu, "Results and analysis for a novel 2×2 channel measurement applied in LTE-R at 2.6 GHz," in *Proc. IEEE WCNC*, Istanbul, Turkey, Apr. 2014, pp. 177–181.

[16] B. Chen and Z. Zhong, "Geometry-based stochastic modeling for MIMO channel in high-speed mobile scenario," *Int. J. Antennas Propag.*, vol. 2012, pp. 184682-1–184682-6, Sep. 2012.

[17] T. Zhou, C. Tao, L. Liu, and Z. Tan, "A semiempirical MIMO channel model in obstructed viaduct scenarios on high-speed railway," *Int. J. Antennas Propag.*, vol. 2014, pp. 287159-1–287159-10, Sep. 2014.

[18] A. Ghazal, C.-X. Wang, B. Ai, D. Yuan, and H. Haas, "A nonstationary wideband MIMO channel model for high-mobility intelligent transportation systems," *IEEE Trans. Intell. Transp. Syst.*, vol. 16, no. 2, pp. 885–897, Apr. 2015.

[19] L. Tian, X. F. Yin, X. Zhou, and Q. Zuo, "Spatial cross-correlation modeling for propagation channels in indoor distributed antenna systems," *EURASIP J. Wireless Commun. Netw.*, vol. 2013, pp. 183-1–183-11, 2013.

[20] T. Zhou, C. Tao, S. Salous, Z. Tan, L. Liu, and L. Tian, "Graph-based stochastic model for high-speed railway cutting scenarios," *IET Microw., Antennas Propag.*, vol. 9, no. 15, pp. 1691–1697, Dec. 2015.

[21] T. Zhou, C. Tao, S. Salous, L. Liu, and Z. Tan, "Channel sounding for high-speed railway communication systems," *IEEE Commun. Mag.*, vol. 53, no. 10, pp. 70–77, Oct. 2015.

[22] B. Chen, Z. Zhong, B. Ai, and D. G. Michelson, "Moving virtual array measurement scheme in high-speed railway," *IEEE Antennas Wireless Propag. Lett.*, vol. 15, pp. 706–709, Mar. 2016.

[23] W. Wang, T. Jost, and A. Dammann, "Estimation and modelling of NLoS time-variant multipath for localization channel model in mobile radios," in *Proc. IEEE GLOBECOM*, Miami, FL, USA, Dec. 2010, pp. 1–6.

[24] E. G. Larsson, O. Edfors, F. Tufvesson, and T. L. Marzetta, "Massive MIMO for next generation wireless systems," *IEEE Commun. Mag.*, vol. 52, no. 2, pp. 186–195, Feb. 2014.

[25] X. Cai, X. F. Yin, and A. P. Yuste, "Direction-of-arrival estimation using single antenna in high-speed-train environments," in *Proc. 10th EuCAP*, Davos, Switzerland, 2016, pp. 1–4.

[26] S. Salous, *Radio Propagation Measurement and Channel Modelling*. West Sussex, U.K.: Wiley, 2013.

[27] O. Renaudin, V.-M. Kolmonen, P. Vainikainen, and C. Oestges, "Non-stationary narrowband MIMO inter-vehicle channel characterization in the 5-GHz band," *IEEE Trans. Veh. Technol.*, vol. 59, no. 4, pp. 2007–2015, May 2010.

[28] D. W. Matolak and R. Sun, "Air–ground channel characterization for unmanned aircraft systems—Part I: Methods, measurements, and models for over-water settings," *IEEE Trans. Veh. Technol.*, vol. 66, no. 1, pp. 26–44, Jan. 2017.

[29] A. Goldsmith, *Wireless Communications*, Cambridge, U.K.: Cambridge Univ. Press, 2005.

[30] M. D. Zoltowski and K. T. Wong, "Closed-form eigenstructure-based direction finding using arbitrary but identical subarrays on a sparse uniform Cartesian array grid," *IEEE Trans. Signal Process.*, vol. 48, no. 8, pp. 2205–2210, Aug. 2000.

[31] X. Cheng, C.-X. Wang, D. I. Laurenson, S. Salous, and A. V. Vasilakos, "An adaptive geometry-based stochastic model for non-isotropic MIMO mobile-to-mobile channels," *IEEE Trans. Wireless Commun.*, vol. 8, no. 9, pp. 4824–4835, Sep. 2009.

[32] X. Cheng, C.-X. Wang, B. Ai, and H. Aggoune, "Envelope level crossing rate and average fade duration of nonisotropic vehicle-to-vehicle ricean fading channels," *IEEE Trans. Intell. Transp. Syst.*, vol. 15, no. 1, pp. 62–72, Feb. 2014.

[33] X. Cheng, Q. Yao, M. Wen, C.-X. Wang, L.-Y. Song, and B.-L. Jiao, "Wideband channel modeling and intercarrier interference cancellation for vehicle-to-vehicle communication systems," *IEEE J. Sel. Areas Commun.*, vol. 31, no. 9, pp. 434–448, Sep. 2013.

[34] A. Abdi and M. Kaveh, "A space-time correlation model for multielement antenna systems in mobile fading channels," *IEEE J. Sel. Areas Commun.*, vol. 20, no. 3, pp. 550–560, Apr. 2002.

[35] X. Yin, X. Cai, X. Cheng, J. Chen, and M. Tian, "Empirical geometry-based random-cluster model for high-speed-train channels in UMTS networks," *IEEE Trans. Intell. Transp. Syst.*, vol. 16, no. 5, pp. 2850–2861, Oct. 2015.

[36] T. Zhou, C. Tao, L. Liu, and Z. Tan, "Ricean K-factor measurements and analysis for wideband high-speed railway channels at 2.35 GHz," *Radioengineering*, vol. 23, no. 2, pp. 578–585, Jun. 2014.

[37] *Sencity Rail Antenna: 1399.17.0039 HUBER+SUHNER Data Sheet, HUBER+SUHNERAG RF Industrial*, 2010. AQ:7

[38] T. Zhou, C. Tao, S. Salous, L. Liu, and Z. H. Tan, "Implementation of an LTE-based channel measurement method for high-speed railway scenarios," *IEEE Trans. Instrum. Meas.*, vol. 65, no. 1, pp. 25–36, Jan. 2016.

[39] R. He, Z. Zhong, B. Ai, J. Ding, Y. Yang, and A. F. Molisch, "Short-term fading behavior in high-speed railway cutting scenario: Measurements, analysis, and statistical models," *IEEE Trans. Antennas Propag.*, vol. 61, no. 4, pp. 2209–2222, Apr. 2013.

[40] K. Guan, Z. Zhong, B. Ai, and T. Kürner, "Propagation measurements and analysis for train stations of high-speed railway at 930 MHz," *IEEE Trans. Veh. Technol.*, vol. 63, no. 8, pp. 3499–3516, Oct. 2014.

[41] R. He, Z. Zhong, B. Ai, G. Wang, J. Ding, and A. F. Molisch, "Measurements and analysis of propagation channels in high-speed railway viaducts," *IEEE Trans. Wireless Commun.*, vol. 12, no. 2, pp. 794–805, Feb. 2013.

[42] M. Haardt and J. A. Nossek, "Unitary ESPRIT: How to obtain increased estimation accuracy with a reduced computational burden," *IEEE Trans. Signal Process.*, vol. 43, no. 5, pp. 1232–1242, May 1995.

[43] T. Zhou, C. Tao, L. Liu, and Z. H. Tan, "A study on a LTE-based channel sounding scheme for high-speed railway scenarios," in *Proc. IEEE 78th VTC-Fall*, Las Vegas, NV, USA, Sep. 2013, pp. 1–5.

[44] M. D. Zoltowski, M. Haardt, and C. P. Mathews, "Closed-form 2-D angle estimation with rectangular arrays in element space or beamspace via unitary ESPRIT," *IEEE Trans. Signal Process.*, vol. 44, no. 2, pp. 316–328, Feb. 1996.

[45] *Generation Partnership Project; Technical Specification Group Radio Access Network; Evolved Universal Terrestrial Radio Access (E-UTRA); Base Station (BS) Radio Transmission and Reception (Release 9)*, 3GPP, document TS 36.104 V9.3.0 3rd, 2010. AQ:8

[46] P. L. Kafle, A. Intarapanich, A. B. Sesay, J. Mcrory, and R. J. Davies, "Spatial correlation and capacity measurements for wideband MIMO channels in indoor office environment," *IEEE Trans. Wireless Commun.*, vol. 7, no. 5, pp. 1560–1571, May 2008.

[47] C. Oestges, D. Vanhoenacker-Janvier, and B. Clerckx, "Wide-band SIMO 1×2 measurements and characterization of outdoor wireless channels at 1.9 GHz," *IEEE Trans. Veh. Technol.*, vol. 53, no. 4, pp. 1190–1202, Jul. 2004.

Tao Zhou (M'16) received the B.E. degree from Changchun University of Science and Technology, Changchun, China, in 2009 and the Ph.D. degree from Beijing Jiaotong University, Beijing, China, in 2016.

From 2014 to 2015, he was a visiting Ph.D. Student with the Centre for Communication Systems, School of Engineering and Computing Sciences, Durham University, U.K. Since 2016, he has been an Associate Professor with Institute of Broadband Wireless Mobile Communications, School of Electronics and Information Engineering, Beijing Jiaotong University. His research interests include propagation channel characterization, channel sounding, and modeling for high-speed railway communication systems.

Cheng Tao (M'95) received the M.S. degree in telecommunication and electronic system from Xidian University, Xian, China, in 1989 and the Ph.D. degree in telecommunication and electronic system from Southeast University, Nanjing, China, in 1992.

He was a Post-Doctoral Fellow with the School of Electronics and Information Engineering, Beijing Jiaotong University (BJTU), Beijing, China, from 1993 to 1995. From 1995 to 2006, he was with the Air Force Missile College and the Air Force Commander College. In 2006, he joined as an Academic Faculty Member with BJTU, where he is currently a Full Professor and the Director of the Institute of Broadband Wireless Mobile Communications. He has authored over 50 papers and holds 20 patents. His current research interests include mobile communications, multiuser signal detection, radio channel measurement and modeling, and signal processing for communications.

Sana Salous (SM'95) received the B.E.E. degree from American University of Beirut, Beirut, Lebanon, in 1978, and the M.Sc. and Ph.D. degrees from Birmingham University, Birmingham, U.K., in 1979 and 1984, respectively. She was an Assistant Professor with Yarmouk University, Irbid, Jordan, for four years. She was a Research Fellow with Liverpool University, Liverpool, U.K., for one year. She held a Lectureship with University of Manchester Institute of Science and Technology, Manchester, U.K., in 1989, where she was subsequently a Senior Lecturer and then a Reader. Since 2003, she has been the Chair in communications engineering with Durham University, Durham, U.K., where she is currently the Director of the Centre for Communication Systems. Her research interests include radio channel characterization in various frequency bands ranging from skywave in the HF band to millimeter bands at 60 GHz, the design of radar waveforms, novel radio channel sounders, and radar systems for radio imaging.

Dr. Salous is a fellow of the Institution of Engineering and Technology. She is the Chair of the Commission C on Radio Communication and Signal Processing Systems of the International Union of Radio Science. She is an Associate Editor of *Radio Science* journal.

Liu Liu (M'12) received the B.E. and Ph.D. degrees from Beijing Jiaotong University (BJTU), Beijing, China, in 2004 and 2010, respectively.

He was a Post-Ph.D. Researcher with the School of Electronics and Information Engineering, Institute of Broadband Wireless Mobile Communications, BJTU, from 2010 to 2012, where he has been an Associate Professor Since 2012. His research interests include channel measurement and modeling for different propagation environments and signal processing of wireless communication in time-varying channel.

AUTHOR QUERIES

AUTHOR PLEASE ANSWER ALL QUERIES

PLEASE NOTE: We cannot accept new source files as corrections for your paper. If possible, please annotate the PDF proof we have sent you with your corrections and upload it via the Author Gateway. Alternatively, you may send us your corrections in list format. You may also upload revised graphics via the Author Gateway.

AQ:1 = Please confirm whether the corresponding authors information is correct as set.
AQ:2 = Please note that there were discrepancies between the accepted pdf [Measurements and Analysis of Angular Characteristics and Spatial Correlation for High-Speed Railway Channels_revised1_print.pdf] and the [Measurements and Analysis of Angular Characteristics and Spatial Correlation for High-Speed Railway Channels.tex] in the inline reference number and reference count. We have followed [Measurements and Analysis of Angular Characteristics and Spatial Correlation for High-Speed Railway Channels.tex].
AQ:3 = Please provide the accessed date for refs. [2] and [3].
AQ:4 = Please confirm the volume no. for refs. [6], [16], [17], and [19].
AQ:5 = Please confirm the author names, article title, and year for ref. [8]. Also provide the journal title, volume no., issue no., page range, and month.
AQ:6 = Please provide the organization, location, and report no. for ref. [14].
AQ:7 = Please confirm the title and year for refs. [37]. Also provide the organization name and organization location.
AQ:8 = Please confirm the title, document no., and year for ref. [45].

Measurements and Analysis of Angular Characteristics and Spatial Correlation for High-Speed Railway Channels

Tao Zhou, *Member, IEEE*, Cheng Tao, *Member, IEEE*, Sana Salous, *Senior Member, IEEE*, and Liu Liu, *Member, IEEE*

***Abstract*— Spatial characteristics of the propagation channel have a vital impact on the application of multi-antenna techniques. This paper analyzes angular characteristics and the spatial correlation for high-speed railway (HSR) channels, based on a novel moving virtual antenna array (MVAA) measurement scheme. The principle of the MVAA scheme is deeply investigated and is further verified by a theoretical geometry-based stochastic model. Using the MVAA scheme, virtual single-input multiple-output (SIMO) channel impulse response data are derived from single-antenna measurements in typical HSR scenarios, involving viaduct, cutting, and station. Based on the SIMO channel data, angle of arrival is extracted according to the unitary estimation of signal parameters by the rotational invariance techniques algorithm, and is compared with the theoretical result. Moreover, power angular spectrum and root mean square (rms) angular spread (AS) are provided, and the rms AS results are statistically modeled and comprehensively compared. In addition, spatial correlation is calculated and analyzed, and a rms AS-dependent spatial correlation model is newly proposed to describe the relationship between the angular dispersion and the spatial correlation. The presented results could be used in multi-antenna channel modeling and will facilitate the assessment of multi-antenna technologies for future HSR mobile communication systems.**

***Index Terms*— High-speed railway channel, virtual antenna array, angualr characteristics, spatial correlation, channel modeling.**

I. Introduction

As WITH the previous generation systems, the upcoming fifth-generation (5G) mobile communication system will cover not only conventional cellular scenarios but also high mobility scenarios, such as highway, subway, and high-speed railway (HSR) [1]. Although 5G aims at delivering a consistent experience across a variety of scenarios, it is a great challenge for 5G solutions to provide a satisfactory service to passengers on high-speed trains at a speed of up to 500 km/h [2]. Thus, the application of 5G techniques in HSR scenarios are attracting more attention.

It is expected that 5G will be able to support 0.1∼1 Gbps user experienced data rate and tens of Gbps peak data rate [3]. In order to meet the requirement of such high AQ:2 data rate, multiple-input multiple-output (MIMO) and massive MIMO [4], which exploit the spatial domain of mobile fading to enhance system capacity, will be the key supporting techniques in 5G. Intuitively, the HSR is not a favorable environment for using multi-antenna techniques, due to the line-of-sight (LOS) dominance [5]. However, there exist a wide variety of propagation scenarios on HSR, such as urban, suburban, rural, hilly, as well as a number of special scenarios like cutting, viaduct, tunnel, station, and so on, some of which could have rich scattering and reflecting components [6]. To apply the multi-antenna techniques on HSR, it is quite necessary to investigate spatial characteristics in various HSR scenarios.

The spatial characteristics of the propagation channel can be classified into two categories: angular characteristics and spatial correlation. The former is an indispensable part in spatial channel modeling, while the latter is a popular parameter to evaluate the performance of multi-antenna techniques. So far, most of the studies have concentrated on the large-scale fading, delay dispersion and frequency dispersion in HSR channels [7]–[11]. However, there are few works referring to the spatial characteristics in the HSR environments. Angular characterization for HSR channel was first presented in [12] where root mean square (RMS) angular spread (AS) was obtained from single-input multiple-output (SIMO) measurements using the relay coverage (RC) scheme. Although the well-known WINNER II model [13] includes the RMS AS result into the D2a scenario which is regarded as a kind of fast train scenario, it does not specify the applicable HSR scenarios, e.g., viaduct, cutting or station. In [14], multi-antenna measurements considering the direct coverage (DC) scheme were conducted for analyzing angle of arrival (AOA) and RMS AS parameters in specific HSR environments, including an agricultural area and a hilly district. However, the angular characteristics derived from the DC measurement

Manuscript received October 17, 2016; revised January 19, 2017 and February 21, 2017; accepted March 2, 2017. This work was supported in part by the National Natural Science Foundation of China under Grant 61371070 and Grant 61471030, in part by the Beijing Natural Science Foundation under Grant 4174102, in part by the Fundamental Research Funds for the Central Universities under Grant 2016RC031, and in part by the Open Research Fund through the National Mobile Communications Research Laboratory, Southeast University, under Grant 2014D05. The Associate Editor for this paper was
AQ:1 X. Cheng. *(Corresponding authors: Liu Liu and Cheng Tao.)*

T. Zhou and L. Liu are with the Institute of Broadband Wireless Mobile Communications, Beijing Jiaotong University, Beijing 100044, China (e-mail: taozhou@bjtu.edu.cn; liuliu@bjtu.edu.cn).

C. Tao is with the Institute of Broadband Wireless Mobile Communications, Beijing Jiaotong University, Beijing 100044, China, and also with the National Mobile Communications Research Laboratory, Southeast University, Nanjing 210096, China (e-mail: chtao@bjtu.edu.cn).

S. Salous is with the School of Engineering and Computing Sciences, Durham University, Durham DH1 3LE, U.K. (e-mail: sana.salous@durham.ac.uk).

Color versions of one or more of the figures in this paper are available online at http://ieeexplore.ieee.org.

Digital Object Identifier 10.1109/TITS.2017.2681112

embody the effect of scatterers and reflectors inside the train carriage, which cannot represent the realistic angular dispersion in the outdoor propagation environment of HSR. Based on a 2×2 MIMO RC measurement in HSR viaduct scenarios, [15] initially discussed the spatial correlation of the HSR channel, which shows that the correlation coefficient varies from a higher value to a lower value as the train moves far away from base station (BS). In addition, some theoretical channel models, such as geometry-based stochastic model (GBSM) [16]–[18] and propagation graph-based model [19], [20], have been used to analyze the spatial characteristics in numerous HSR environments. Although the theory-based models are convenient for the analysis and simulation of the multi-antenna channel, they still need the support of actual measurement data.

It is well-known that performing multi-antenna channel measurements on HSR is highly difficult because of some measurement constraints [21]. The lack of multi-antenna measurement data leads to a huge gap of the spatial characteristics on HSR multi-antenna channel modeling and performance evaluation. To overcome the difficulty of the HSR multi-antenna channel measurements, a moving virtual antenna array (MVAA) measurement scheme has been proposed and verified in [22], which employs a single antenna to simulate multiple virtual antennas. A similar scheme was applied in MIMO and massive MIMO measurements for indoor static scenarios [23], [24]. According to the MVAA scheme, AOA estimation was implemented based on single-antenna measurements in HSR viaduct scenarios [25]. However, the specific HSR spatial characteristics are not given.

To fill the aforementioned research gaps, this paper provides detailed analysis of angular characteristics and spatial correlation in typical HSR scenarios, involving viaduct, cutting, and station. The major contributions and novelties of this paper are as follows.

1) The MVAA scheme is deeply investigated and is further verified by a GBSM from the theoretical perspective. According to single-antenna measurements and the validated MVAA scheme, virtual SIMO channel data in the three HSR scenarios are generated for spatial characterization.

2) The AOA and power angular spectrum (PAS) are extracted depending on the virtual SIMO channel data. The RMS AS is obtained and statistically modeled, and compared in various HSR scenarios. The acquired RMS AS results will be useful for HSR multi-antenna channel modeling.

3) The spatial correlation in the three HSR environments is analyzed, and the RMS AS-dependent spatial correlation model is proposed to describe the relationship between the angular dispersion and the spatial correlation, which will facilitate HSR multi-antenna technique evaluation.

The remainder of this paper is outlined as follows. Section II highlights the MVAA measurement scheme. In Section III, the virtual SIMO measurement data are acquired. Angular characteristics and spatial correlation are presented in Section IV and Section V, respectively. Finally, conclusions are drawn in Section VI.

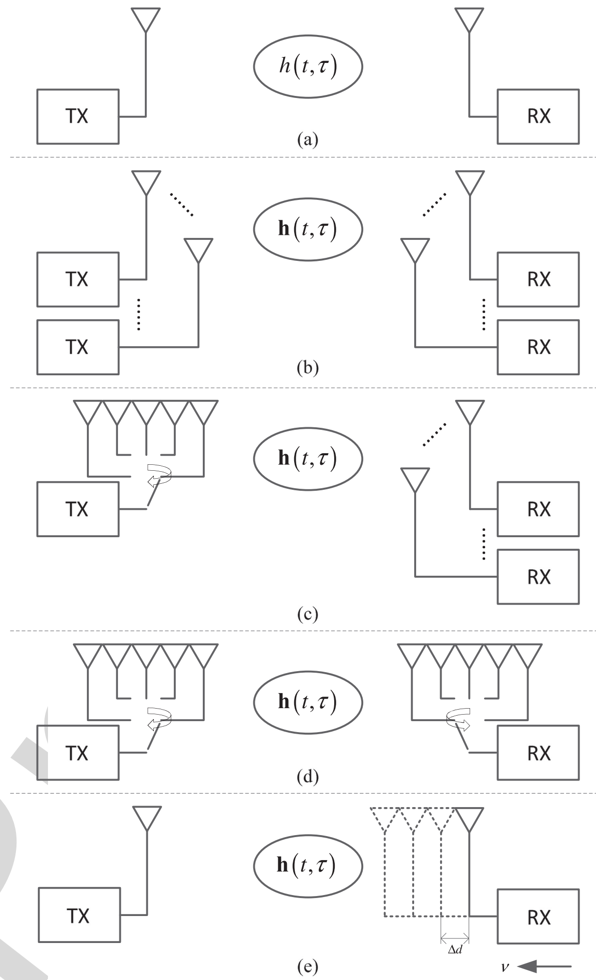

Fig. 1. Channel sounding schemes. (a) SISO scheme. (b) Full parallel scheme. (c) Semi-sequential scheme. (d) Fully sequential scheme. (e) MVAA scheme.

II. Moving Virtual Antenna Array Measurement Scheme

A. Principle

In radio channel sounding, a known signal that repeats at a rate twice the highest expected Doppler shift is transmitted, and the received signal is analyzed to extract the channel impulse response (CIR). The SISO channel sounding scheme that employs a single transmitter (TX) and a single receiver (RX) is most commonly used, as displayed in Fig. 1(a). For conventional multi-antenna channel sounding schemes, they can be classified into three categories [26], as shown in Fig. 1(b)-(d): 1) Full parallel scheme at both the TX and at the RX using a number of orthogonal techniques such as code division multiplexing (CDM) and frequency division multiplexing (FDM); 2) Semi-sequential scheme with time division multiplexing (TDM) at the TX only with parallel receive channels; 3) Fully sequential scheme with TDM at both ends of the link. The full parallel scheme is capable of measuring time-variant channels without restriction. However, for TDM schemes, due to the sequential nature of the measurement, the time required to complete a single sequential measurement depends on the size of the arrays and the repetition time of the sounding waveform. Such sequential measurements should ensure that the channel is either stationary or quasi-stationary during the time of the measurement.

According to the idea of the sequential measurement, a novel MVAA scheme with the advantages of low-cost and low-complexity is proposed, as shown in Fig. 1(e). The proposed scheme employs the hardware that is the same as applied in the SISO scheme. In addition, it does not require fast switches that have to be used in the semi-sequential or fully sequential scheme to control the antenna arrays. When the TX is static and the RX is moving toward the TX with a stable speed, the neighboring samples of the measured CIR can be regarded as several virtual antenna elements. These virtual antenna elements are distributed equally and form a uniform linear array (ULA) with the direction parallel to the moving track. In order to generate the ULA, two important parameters, the element spacing and the element number, should be known.

The element spacing of the ULA is related to the moving speed υ and the repetition time of the sounding waveform T_{rep}, expressed as

$$\Delta d = \upsilon T_{rep}. \tag{1}$$

In general, there are two solutions used to determine Δd, including speed-sensor solution and GPS solution. Here, the speed-sensor solution is recommended because of the higher precision.

On the other hand, the element number of the ULA in the MVAA scheme should be limited. To enable the MVAA scheme, the basic criterion is that the channel should be constant in the duration of the samples which are used to generate the ULA. Thus, the duration that refers to the element number of the ULA M and T_{rep} should be no more than the channel coherence time T_c, expressed as

$$(M-1)\cdot T_{rep} \le T_c. \tag{2}$$

In Equation (2), the coherence time is used to quantify the element number. In fact, stationarity distance (SD) which has been presented in [27] for the V2V channel and [28] for the air-ground channel is more appropriate than the coherence time. The SD is the duration over which the channel can be assumed stationarity, and it includes not only Doppler shift, but also LOS condition, multipath and more channel effects. However, it is known that the SD for the HSR channel is still unknown. Thus, this paper only simply consider the coherence time.

Assuming that $T_c = 1/B_d$ [29], where $B_d = 2f_{\max}$ is the Doppler spread, $f_{\max} = \upsilon/\lambda$ is the highest Doppler shift, and λ is the wavelength, Equation (2) is rewritten as

$$M \le 1 + \frac{1}{2\cdot f_{\max} T_{rep}} = 1 + \frac{\lambda/2}{\Delta d}. \tag{3}$$

From Equation (3), M is inversely proportional to Δd, which means that the smaller the duration of the samples is, the more virtual antenna elements can be included in the ULA. In addition, the maximum Δd cannot exceed $\lambda/2$ so that a minimum two-element ULA can be established. If $\Delta d > \lambda/2$, $M = 1$ and the MVAA scheme would be invalid. On the other hand, $\Delta d > \lambda/2$ would lead to a set of cyclically ambiguous AOA estimates, in accordance with the spatial Nyquist sampling theorem [30]. Thus, to achieve the MVAA scheme, $\Delta d \le \lambda/2$ should be satisfied.

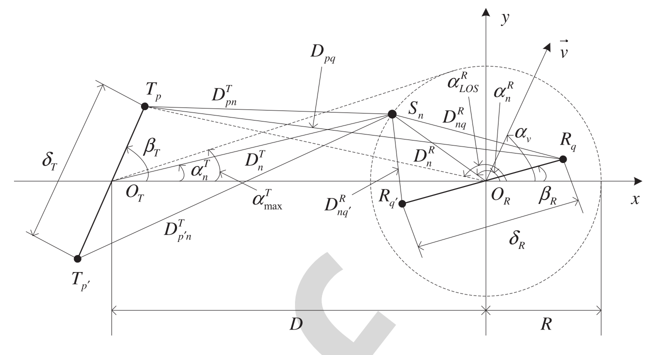

Fig. 2. A 2×2 GBSM with one-ring architecture.

B. Validation

In order to validate the MVAA scheme, a 2×2 GBSM with the classical one-ring architecture is considered, as shown in Fig. 2 [31]. The RX is surrounded by local scatterers S_n, $n = 1, 2, \ldots, N$. The TX and RX antenna element spacings are denoted by δ_T and δ_R, and the tilt angles of the arrays are represented by β_T and β_R, respectively. The ring radius is R and the distance between TX and RX is D. The angle-of-motion α_υ indicates the angle between the x-axis and the direction of motion with the speed of υ. The symbol $\alpha^T_{\max}$ stands for the maximum AOD seen from the TX. This quantity is related to R and D by $\alpha^T_{\max} = \arctan(R/D) \approx R/D$. Moreover, it is assumed that both R and D are large compared to the geometrical size of the antenna arrays, i.e., $D \gg R \gg \max\{\delta_T, \delta_R\}$.

According to the established GBSM, the closed-form expression of space-time (ST) correlation function (CF) between two subchannels $h_{pq}(t)$ and $h_{p'q'}(t)$ can be derived by [32], [33]

$$\rho_{h_{pq},h_{p'q'}}(\delta_T, \delta_R, \tau) = \frac{E\left[h_{pq}(t)\, h^*_{p'q'}(t+\tau)\right]}{\sqrt{\Omega_{pq}\Omega_{p'q'}}}, \tag{4}$$

where Ω_{pq} and $\Omega_{p'q'}$ denote the total power of the T_p-R_q link and $T_{p'}$-$R_{q'}$ link, and $(\cdot)^*$ indicates the complex conjugate.

In case of isotropic scattering, substituting $\delta_T = \delta_R = 0$ and $\tau = 0$ into the closed-form expression of ST CF, the time CF and the space CF can be respectively obtained as [34]

$$\rho_{h_{pq},h_{p'q'}}(0, 0, \tau) = J_0(2\pi f_{\max}\tau), \tag{5}$$

and

$$\begin{aligned}\rho_{h_{pq},h_{p'q'}}&(\delta_T, \delta_R, 0)\\ &= e^{j2\pi\frac{\delta_T}{\lambda}\cos(\beta_T)} J_0(2\pi\{(\frac{\delta_R}{\lambda})^2\\ &\qquad + (\frac{\delta_T}{\lambda}\alpha^T_{\max}\sin\beta_T)^2\\ &\qquad + 2\frac{\delta_T\delta_R}{\lambda^2}\alpha^T_{\max}\sin\beta_T\sin\beta_R\}^{1/2}),\end{aligned} \tag{6}$$

where $J_0(\cdot)$ denotes the zeroth-order Bessels function of the first kind.

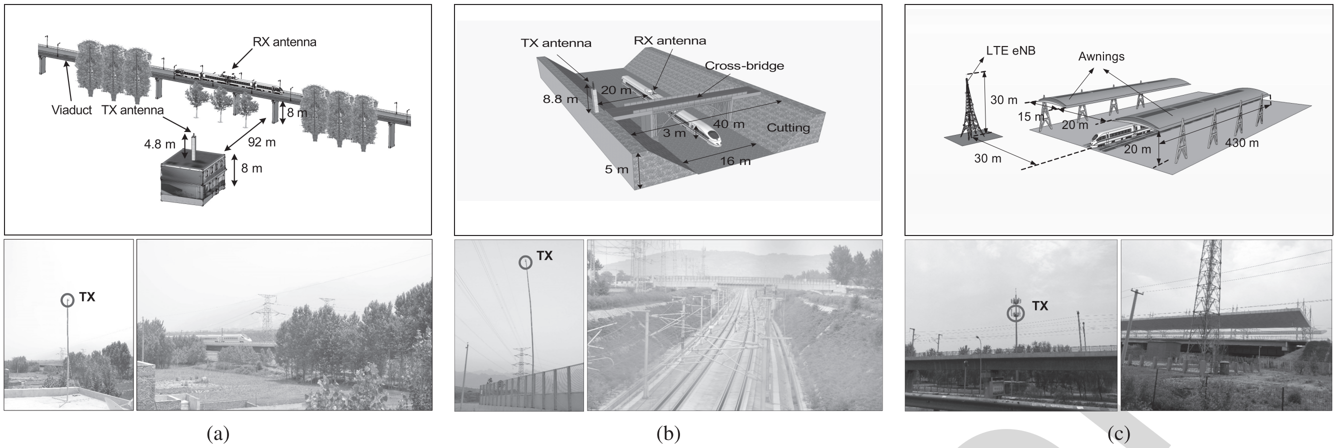

Fig. 3. Overview of the measured scenarios. (a) Viaduct. (b) Cutting. (c) Station.

TABLE I
MEASUREMENT CONFIGURATION

Scenario	Viaduct	Cutting	Station
Equipment	Propsound	Propsound	LTE Sounder
Carrier frequency	2350 MHz	2350 MHz	1890 MHz
TX power	30.8 dBm	32.7 dBm	CRS: 12.2 dBm
Bandwidth	50 MHz	50 MHz	18 MHz
Waveform repetition frequency	1968.5 Hz	1968.5 Hz	2000 Hz
TX antenna height	12.8 m	13.8 m	30 m
RX antenna height	11 m	3 m	10 m
Distance between TX and railway track	92 m	30 m	30 m
Train velocity	198 km/h	198 km/h	285 km/h

Applying the MVAA scheme to the GBSM model, i.e., setting $\delta_T = 0$ and $\delta_R = \Delta d$, the space CF is transformed into

$$\rho_{h_{pq},h_{p'q'}}(0, \Delta d, 0) = J_0\left(2\pi v T_{rep}/\lambda\right) = \rho_{h_{pq},h_{p'q'}}(0, 0, \tau). \quad (7)$$

Equation (7) shows that according to the MVAA scheme, the space CF in the GBSM model equals the time CF. This confirms that the temporal correlation can be equivalent to the spatial correlation by using the MVAA scheme. Thus, it is possible to employ the single-antenna measurement data to perform the analysis of spatial characteristics. In the next section, the virtual multi-antenna measurement data will be generated based on realistic single-antenna measurements and the validated MVAA scheme.

III. VIRTUAL SIMO MEASUREMENT DATA

A. Measurement Campaigns

Both positive and passive sounding approaches [35] are employed in the single-antenna channel measurements for three typical HSR scenarios. Propsound, a positive channel sounder, is used to conduct RC channel measurements in viaduct and cutting scenarios on Zhengzhou to Xi'an HSR in China [36]. The TX equipped with a vertical-polarized dipole antenna is placed near the railway track to send out an excitation signal. The RX is positioned inside the train carriage and employs a special train-mounted antenna, HUBER+SUHNER [37], to collect the test signal. In addition, a passive long-term evolution (LTE) sounder is employed to perform RC measurements in a station scenario on Beijing to Tianjin HSR in China [38]. The LTE eNodeB (eNB) in the specialized railway network transmits LTE signal by a directional antenna. The LTE sounder utilizes the HUBER+SUHNER antenna to collect the LTE signal and extracts CIR from cell-specific reference signal (CRS). The specific measurement configuration for the three scenarios is listed in Table I. The measured scenarios are shown in Fig. 3, which have some special features as follows.

1) Viaduct: There are some obvious local scatterers around the viaduct, such as dense trees which are much higher than the train-mounted antenna. These local scatterers will hinder the propagation of radio waves and result in serious channel dispersion. The height of TX antenna is not dominant compared to the RX antenna due to the limited test condition. In this case, the effect of shadowing will be further intensified.

2) Cutting: There are few obstacles in the cutting that seems a semi-closed structure with steep walls on both sides of the railway track. However, since the slopes are usually covered by vegetation, they will produce a great deal of extra reflections and scattering. Moreover, the RX is lower than the steep walls leading to a deep cutting scenario which leads to more multipath components [39]. Especially, there exists a cross-bridge used for setting the TX antenna, which could result in short term blockage of the propagation path.

3) Station: The train with 200-m length, 4-m height, and 3-m width is running through the station under a viaduct with 10-m height. The measured station can be regarded as an open-type station in which the awnings only cover the platform

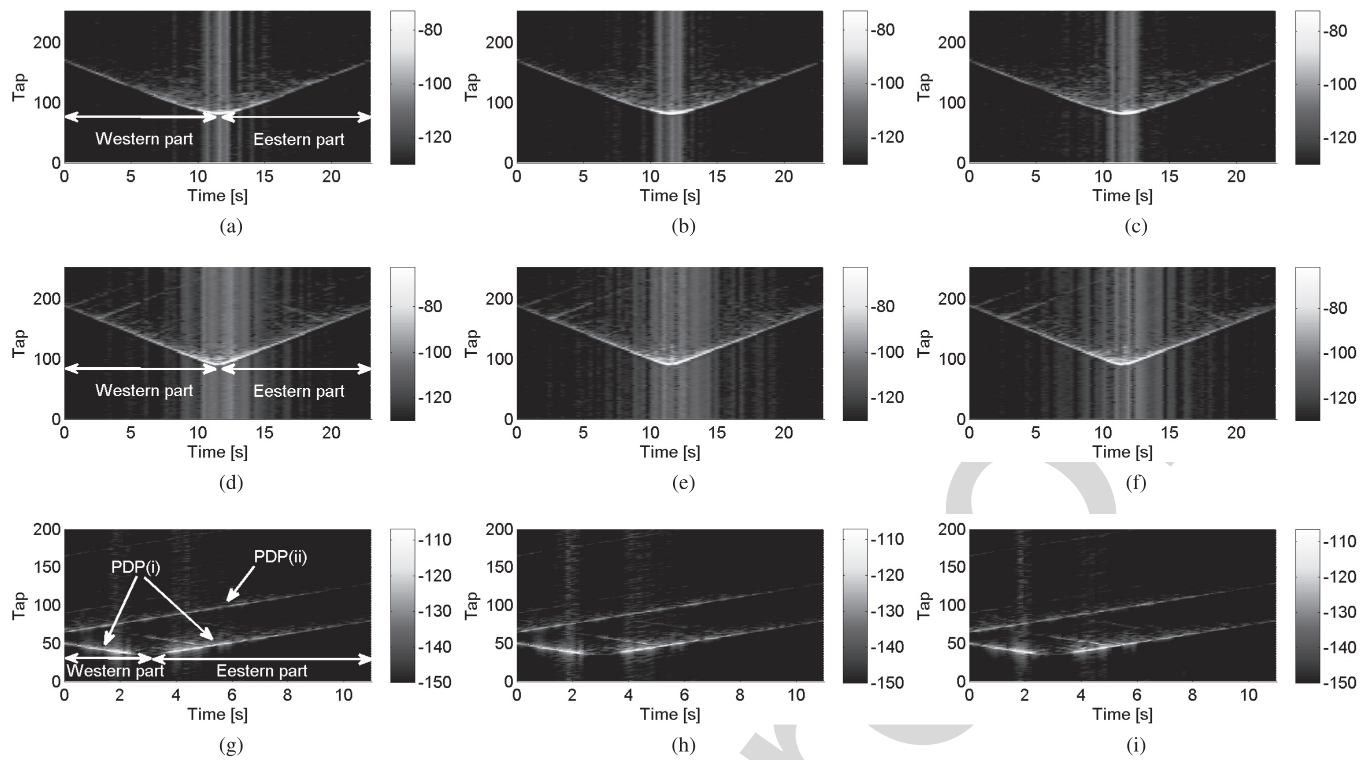

Fig. 4. Time-variant PDPs for h_1, h_2, h_3 in different scenarios. (a-c) Viaduct. (d-f) Cutting. (g-i) Station.

supporting a clear free space over the rail [40]. However, the awnings can still produce lots of scattering and reflections to complicate the fading behavior.

B. Data Processing

The CIR is continuously captured by Propsound and the LTE sounder at a certain interval. This interval is inversely proportional to the waveform repetition frequency (WRF) that should be at least twice the maximum expected Doppler shift. In the viaduct and cutting scenarios, the used CIR data contain 45108 snapshots with a time interval of 0.51-ms, corresponding to 22.9-s duration. In the station environment, the analyzed CIR data consist of 22010 snapshots with a time interval of 0.5-ms, corresponding to 11-s duration. Each snapshot comprises the multipath taps of 254 for the Propsound measurement and 200 for the LTE sounder measurement.

Substituting the values listed in Table I into Equation (3), $M < 3.28$ for the viaduct and cutting scenarios and $M < 3.01$ for the station scenario, which indicates that the virtual array can support a maximum of three elements. Here, the speed-sensor solution is considered and the stable train speed is assumed. Then the three-element virtual ULA with the spacing of 0.22λ and 0.25λ for Propsound and LTE sounder measurements is respectively generated. The CIR from the TX to the m-th virtual receive element ($m = 1, 2, 3$) is derived by

$$h_m(t, \tau) = h(t_{3k+m}, \tau), \quad k = 0, 1, 2... \tag{8}$$

Finally, the multiple-antenna channel data $\mathbf{h}(t, \tau) = [h_1(t, \tau)\ \ h_2(t, \tau)\ \ h_3(t, \tau)]$ are obtained, which can be used for the spatial characterization.

Fig. 4 illustrates the time-variant power delay profiles (PDPs) for h_1, h_2, h_3 in the measured three HSR scenarios. The unit in the colorbars of Fig. 4 is dB. In the viaduct and cutting scenarios, the strongest LOS component is observed when the RX is closest to the TX at around 11.5-s and its power becomes weaker as the RX moves far away from the TX. The whole measurement data can be divided into two parts, the western part and the eastern part. As for the station scenario, two obvious PDP transitions, PDP(i) and PDP(ii), are found in the measurement. The PDP(i) belongs to the propagation channel from the primary eNB to the sounder, whereas the CIR(ii) is caused by the neighboring eNB. The PDP(i) and PDP(ii) can be distinguished in the delay domain according to the method mentioned in [38]. Here, only PDP(i) is used to extract the spatial characteristics. Regarding the PDP(i), the power of the multipath components is weaker when the RX is closest to the TX at around 3-s. This is because the train is underneath the eNB antenna, and the RX is not in the mainlobe of the antenna pattern of the directional antenna [41]. Similar to the viaduct and cutting scenarios, the PDP(i) data in the station measurement can be also classified into the western part and the eastern part.

IV. Results and Discussions

A. Angle of Arrival Estimation

The estimation of signal parameters by the rotational invariance techniques (ESPRIT) algorithm which creates the signal subspace and then extracts the angle information in closed form is capable of analyzing the AOA in azimuth at the RX side. Comparing various ESPRIT algorithms, Unitary ESPRIT [42], [43] is employed due to the lower complexity

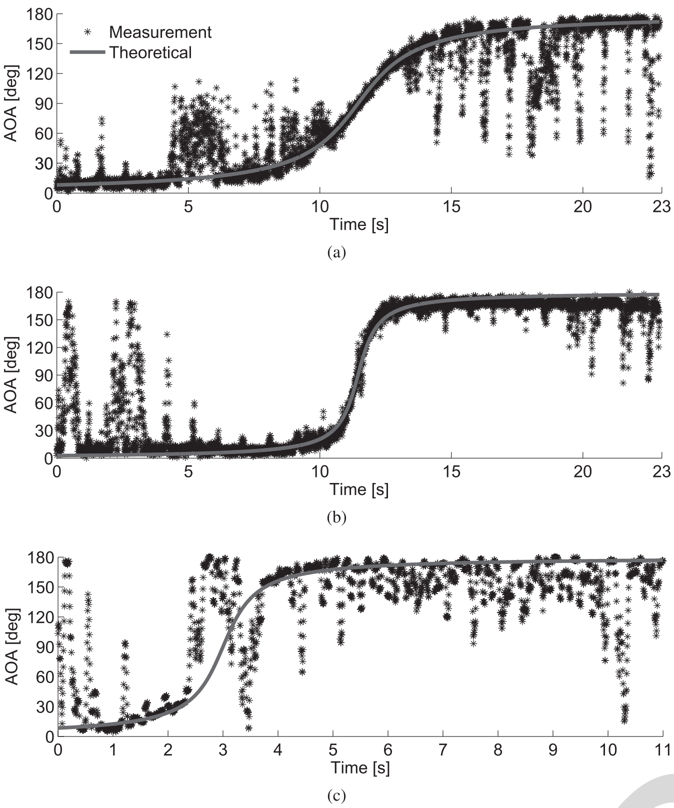

Fig. 5. Time-variant AOAs in different scenarios. (a) Viaduct. (b) Cutting. (c) Station.

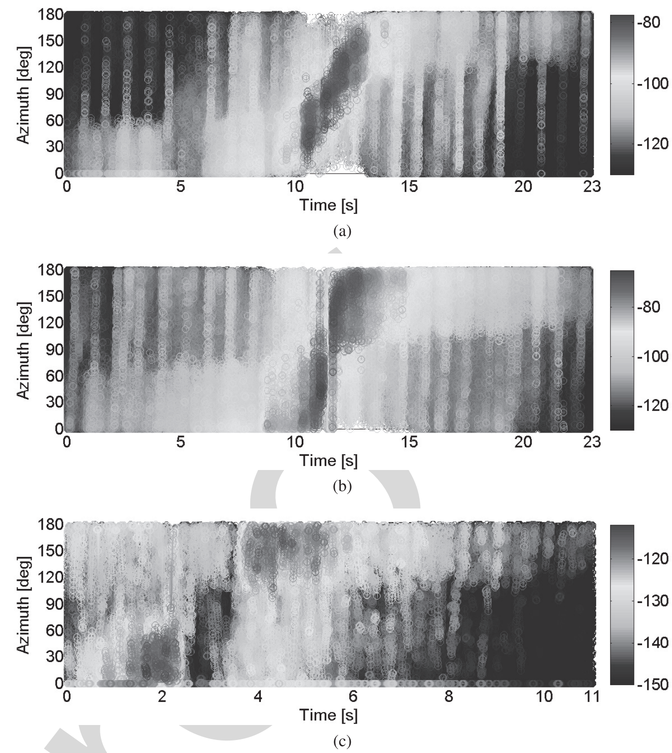

Fig. 6. Instantaneous PASs in different scenarios. (a) Viaduct. (b) Cutting. (c) Station.

and higher accuracy. For the usage of the common Unitary ESPRIT, there are two restrictions: 1) the antenna array should be ULA, otherwise 2-D Unitary ESPRIT algorithms are required [44]; 2) the number of incident waves whose direction can be estimated should be less than the amount of antenna array elements. Since the three-element ULA is generated in the virtual SIMO measurements, the simple 1-D Unitary ESPRIT can be used. However, due to the limited element number of the MVAA, only one or two incident waves for each cluster can be identified. Such low resolution leads to the difficulty of analyzing the cluster-wise angle information. Thus, this paper mainly concentrates on the global angle parameters which are also of interest in the geometric MIMO channel modeling [14].

The Unitary ESPRIT algorithm is applied to the virtual SIMO measurement data $h(t, \tau_l)$ and provides the estimate of AOA associated with the l-th delay. Fig. 5 shows the AOA results for the strongest cluster in the three scenarios. The theoretical AOA for the LOS condition, as a reference, is also shown in Fig. 5. In [45], the theoretical time-varying AOA is given as

$$\hat{\theta}(t) = \arccos\left\{\frac{\upsilon(t_0 - t)}{\sqrt{d_{\min}^2 + [\upsilon(t - t_0)]^2}}\right\}, \quad 0 \le t \le t_0, \tag{9}$$

where $d_{\min}$ denotes the minimum distance between TX and RX, i.e., the distance between the train and the railway track. t_0 represents the moment when the TX passes by the RX, i.e., when the distance between TX and RX equals $d_{\min}$.

It is observed from Fig. 5 that there is a good match between the measured and theoretical results with regard to the overall AOA variation. The AOA changes approximately from 0° to 180° due to the impact of the movement of the train. Since the TX in the cutting or station scenarios is much closer to the railway track, the variation in the cutting or station scenarios is faster than that in the viaduct scenario when the train passes through the TX. It is also found that the AOA values in some regions have a larger deviation from the theoretical results. This is because there are non-LOS (NLOS) clusters appearing in the regions, such as the coverage areas of the dense trees in the viaduct scenario, the cross-bridge in the cutting scenario, and the awnings in the station scenario. Furthermore, it is seen that there is a dramatic fluctuation around 3-s in the station scenario since the train is located in the sidelobe of the directional antenna.

B. Power Angular Spectrum

Using the estimated AOAs, an array steering matrix can be formed. For the ULA, the array steering matrix can be constructed as

$$\mathrm{A}_{\Theta} = \begin{bmatrix} 1 & 1 & \cdots & 1 \\ e^{j\frac{2\pi\,\Delta d \sin\theta_1}{\lambda}} & e^{j\frac{2\pi\,\Delta d \sin\theta_2}{\lambda}} & \cdots & e^{j\frac{2\pi\,\Delta d \sin\theta_P}{\lambda}} \\ \vdots & \vdots & \ddots & \vdots \\ e^{j\frac{2\pi(M-1)\Delta d \sin\theta_1}{\lambda}} & e^{j\frac{2\pi(M-1)\Delta d \sin\theta_2}{\lambda}} & \cdots & e^{j\frac{2\pi(M-1)\Delta d \sin\theta_P}{\lambda}} \end{bmatrix}, \tag{10}$$

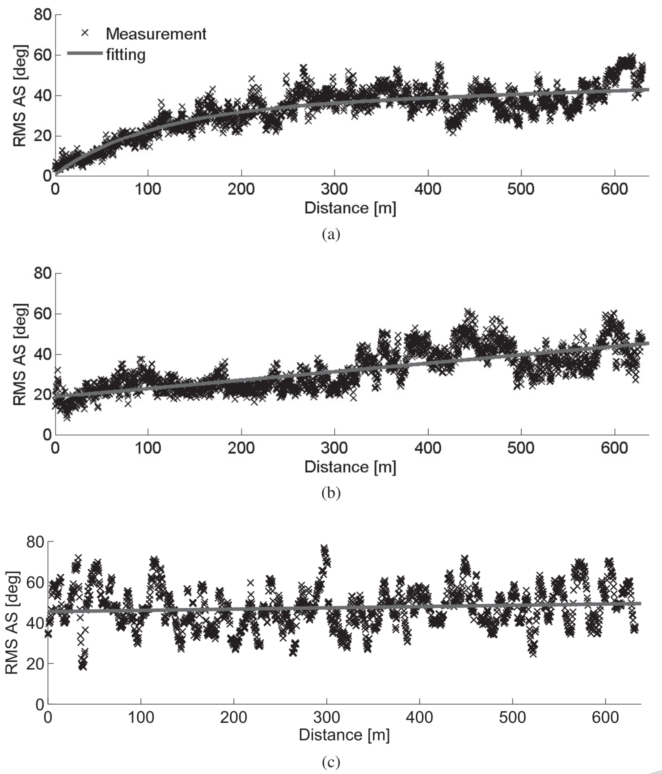

Fig. 7. Distance-dependent RMS AS in different scenarios. (a) Viaduct. (b) Cutting. (c) Station.

where P is the number of identifiable incident waves, P should be smaller than M, and $\Theta = \{\theta_1, \theta_2, \cdots, \theta_P\}$ is the set of the estimated AOAs. Subsequently, the Moore-Penrose pseudoinverse of A_Θ (denoted as $\mathrm{A}_\Theta^\dagger = \left(\mathrm{A}_\Theta^H \mathrm{A}_\Theta\right)^{-1} \mathrm{A}_\Theta^H$) is used to obtain the estimates of incident waves corresponding to the set of AOAs as [46]

$$\begin{aligned} h_\Theta(t, \tau_l) &= \mathrm{A}_\Theta^\dagger h_m(t, \tau_l) \\ &= \left\{h_{\theta_1}(t, \tau_l), h_{\theta_2}(t, \tau_l), \ldots, h_{\theta_P}(t, \tau_l)\right\}. \end{aligned} \quad (11)$$

Based on the extracted AOAs and the corresponding power, the PAS that characterizes how much power arrives on average from a certain angle can be obtained as [47]

$$P_A(t, \theta) = E\left\{\left|\int\int h(t, \tau, \theta)\, d\theta d\tau\right|^2\right\}. \quad (12)$$

Fig. 6 illustrates the instantaneous PAS results in the three scenarios. The unit in the colorbars of Fig. 6 is dB. It is found that the PAS shows a certain spread in all three scenarios. This is due to the presence of the reflectors and scatterers in the measured scenarios, such as dense trees, steep walls, and awnings. These reflectors and scatterers would produce a number of multipath components with different AOAs, thus leading to angular dispersion. In order to specifically characterize the angular dispersion, RMS DS will be extracted and analyzed in the following subsection.

TABLE II
PARAMETERS OF THE RMS AS MODEL

Scenario	Viaduct	Cutting	Station
x_1	34.19	18.78	45.43
y_1	0.00035	0.041	0.0063
x_2	-33.65	-	-
y_2	-0.0095	-	-
σ_θ	5.78	6.63	10.1

C. Angular Spread

The RMS AS is calculated as the root second central moment of the PAS

$$\Delta\theta(t) = \sqrt{\frac{\int\left[\theta(t) - \bar{\theta}(t)\right]^2 P_A(t, \theta)\, d\theta}{\int P_A(t, \theta)\, d\theta}}, \quad (13)$$

where $\bar{\theta}(t)$ is the averaged AOA, expressed as

$$\bar{\theta}(t) = \frac{\int \theta(t)\, P_A(t, \theta)\, d\theta}{\int P_A(t, \theta)\, d\theta}. \quad (14)$$

The relationship between the channel parameters and the distance is always of interest in channel characterization [47]. Here, $\Delta\theta(t)$ is transformed into the value as a function of the distance $\Delta\theta(d)$, where d denotes the relative horizontal distance between the TX and the RX. Fig. 7 shows the distance-dependent RMS AS results in the three scenarios. It is worth noting that the results in the viaduct and cutting scenarios are the averaged values derived from both the western half and the eastern half of CIR data, whereas the result in the station scenario is only obtained by the eastern half of CIR(i) data. It can be seen that the RMS AS experiences a gradual growth with the distance in the viaduct and cutting scenarios, which means that more clusters that cause the larger AS can be identified as the distance increases. However, the RMS AS remains almost stable in the station scenario. This is because the train is always within the station where the scattering and reflecting conditions are stationary.

To describe the variation of RMS AS, a double exponential function and two linear functions are employed to fit the RMS AS curves using the least square (LS) method in the viaduct, cutting, and station scenarios, respectively, expressed as

$$\Delta\theta'(d) = \begin{cases} x_1 e^{y_1 d} + x_2 e^{y_2 d}, & \text{viaduct} \\ x_1 + y_1 d, & \text{cutting/station.} \end{cases} \quad (15)$$

Then, a distance-dependent statistical model for the RMS AS results is proposed as

$$\Delta\theta(d) = \Delta\theta'(d) + x\sigma_\theta, \quad (16)$$

where $\Delta\theta'(d)$ denotes the mean value of the RMS AS model, x_1, y_1, x_2 and y_2 are the coefficients of the model, σ_θ indicates the standard deviation of the model, and x represents zero-mean Gaussian variable with the unit standard deviation. The model parameters are listed in Table II.

Fig. 8 depicts the cumulative distribution function (CDF) measurement and Normal fitting results of RMS AS in the three scenarios. A detailed comparison of the statistical RMS AS results in the RC and DC schemes for the viaduct, cutting,

TABLE III
COMPARISON OF THE STATISTIC RMS AS RESULTS IN DIFFERENT HSR SCENARIOS

Scenario	Viaduct	Cutting	Station	D2a [13]	Agricultural Area [14]	Hilly District [14]
Coverage scheme	RC	RC	RC	RC	DC	DC
10% of CDF	15.2°	20.8°	34.5°	21.3°	-	-
50% of CDF	34.7°	29.9°	47.8°	30.4°	-	-
90% of CDF	45.6°	46.3°	60.5°	45.9°	-	-
Mean value	32.7°	31.9°	47.4°	32.5°	75°	60°
Standard deviation	12.9°	10.1°	10.2°	-	-	-

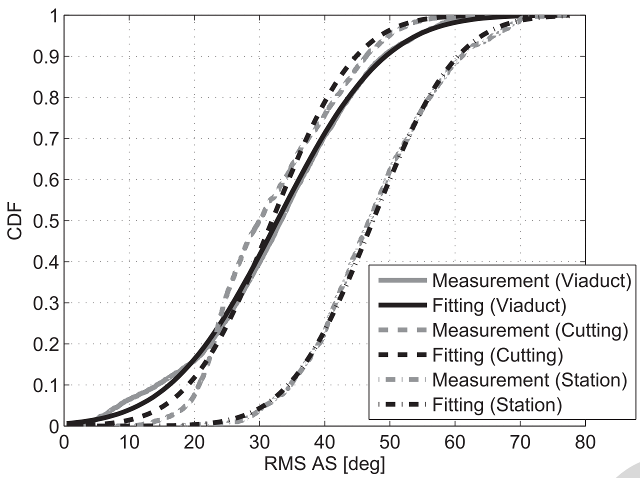

Fig. 8. CDFs of RMS AS in viaduct, cutting and station scenarios.

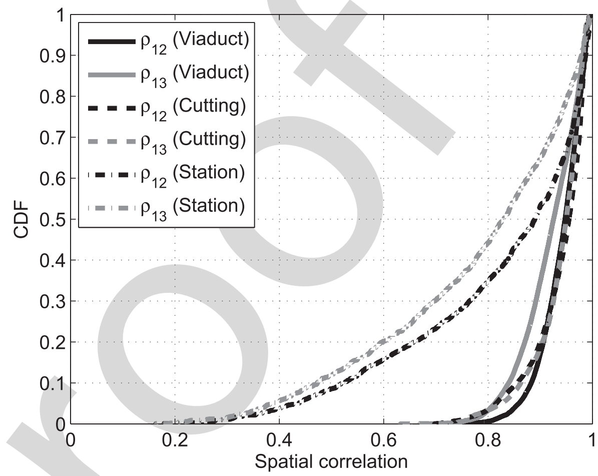

Fig. 9. CDFs of spatial correlation in viaduct, cutting and station scenarios.

station, D2a, agricultural area and hilly district scenarios is shown in Table III. It is observed that the mean value of RMS AS measured in the RC scheme is much smaller than the result obtained in the DC scheme. This confirms that the indoor environment of the train causes additional scattering and reflecting waves, leading to the larger AS. For the RC scheme, it is found that the RMS AS value in the station scenario is much higher than the results in the viaduct, cutting, and D2a scenarios. This is because the station causes more multipath components than the other scenarios. In addition, although 10% and 50% values of RMS AS in the viaduct scenario are respectively lower and higher than those in the cutting scenario, there are similar mean values and 90% values. This means that the measured viaduct scenario with the coverage of dense trees could have the equivalent propagation effect to the cutting scenario as a whole.

D. Spatial Correlation

Spatial correlation between different antenna elements at both ends of the individual link is a key parameter of performance evaluation in MIMO channels. In order to extract the spatial correlation, the wideband data are transformed into the narrowband data $\mathbf{h}(t)$ by making the complex sum of $\mathbf{h}(t,\tau)$ over the delay domain. Then, applying Equation (4) to $\mathbf{h}(t)$, ρ_{12} and ρ_{13} that represent the correlation between $h_1(t)$ and $h_2(t)$ and the correlation between $h_1(t)$ and $h_3(t)$ can be obtained respectively.

Fig. 9 depicts CDF results of ρ_{12} and ρ_{13} with the spacing of $\Delta d_{12} = 0.22\lambda$ and $\Delta d_{13} = 0.44\lambda$ in the viaduct and cutting scenarios and with the spacing of $\Delta d_{12} = 0.25\lambda$ and $\Delta d_{13} = 0.5\lambda$ in the station scenario. It is observed that the spatial correlation in the station scenario is apparently lower than those in the viaduct and cutting scenarios. This confirms that the scattering and reflecting components in the station scenario are much richer. It can be also seen that the correlation decreases as the antenna spacing increases in the three scenarios. Furthermore, 35%~45% values of correlation are lower than 0.8 in the station scenario when $\Delta d \leq 0.5\lambda$, whereas up to 95% values are higher than 0.8 in the viaduct and cutting scenarios. Thus, it is suggested that in case of $\Delta d \leq 0.5\lambda$, the multi-antenna techniques can be used in the station scenario while it is not suitable in the viaduct and cutting scenarios.

TABLE IV
PARAMETERS OF THE SPATIAL CORRELATION MODEL

Scenario	Viaduct	Cutting	Station
a	-2.73e-5	-2.01e-5	-
b	-0.00053	-0.0016	-0.0045
c	0.99	1.01	1.01
σ_ρ	0.036	0.039	0.18

In most of the reported work, the spatial correlation and the RMS AS are always separately considered. In fact, there is a close relation between the spatial correlation and the RMS AS, as illustrated in Fig. 10. It is noted that the spatial correlation decreases with the increase of the RMS AS in the three scenarios. In order to quantitatively describe the relation of the two parameters, a RMS AS-based spatial correlation

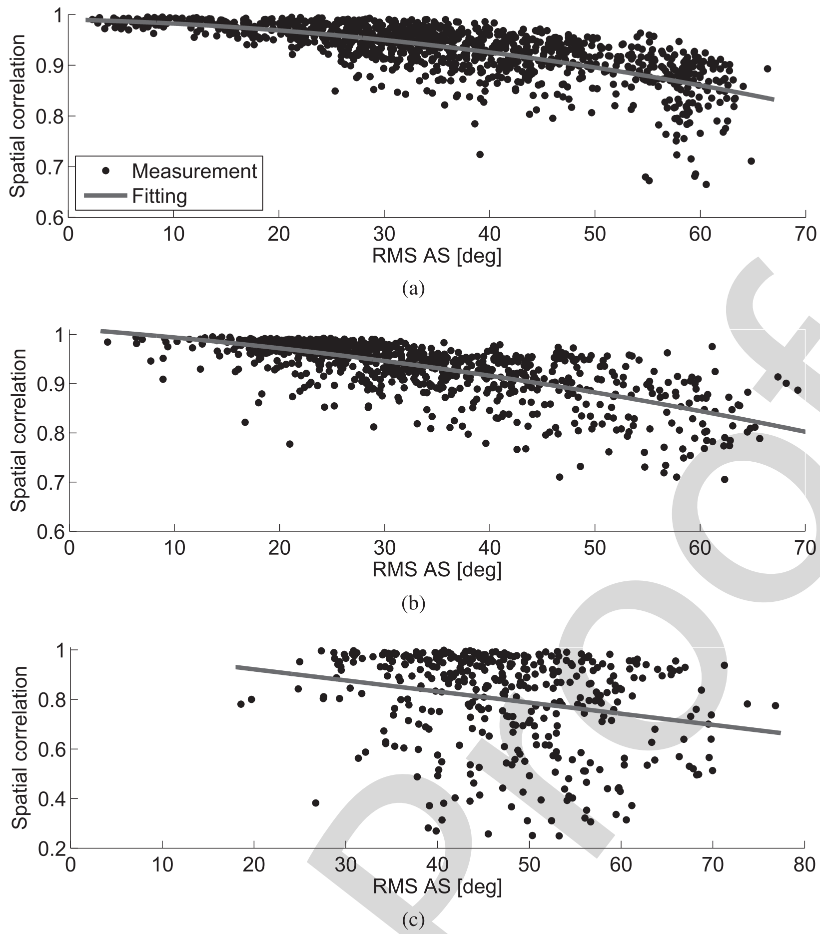

Fig. 10. RMS AS-dependent spatial correlation in different scenarios. (a) Viaduct. (b) Cutting. (c) Station.

model is established as

$$\rho\left(\Delta\theta\right)=\begin{cases}a\Delta\theta^2+b\Delta\theta+c+y\sigma_\rho, & \text{viaduct/cutting}\\ b\Delta\theta+c+y\sigma_\rho, & \text{station,}\end{cases} \quad (17)$$

where, a, b, and c denote the model parameters, σ_ρ indicates the standard deviation of the model, and y represents zero-mean Gaussian variable with the unit standard deviation. The model coefficients are listed in Table IV. Using the proposed spatial correlation model, it could be convenient to determine the spatial correlation coefficient based on the RMS AS value, and then it is possible to evaluate the MIMO performance depending on the RMS AS results.

V. Conclusion

This paper presents the analysis of the angular characteristics and spatial correlation in the HSR viaduct, cutting and station scenarios. The multi-antenna CIR data obtained according to the validated MVAA scheme and the SISO measurements are used for the spatial characterization. It is shown that the AOA estimated by the Unitary ESPRIT algorithm has a reasonable consistency with the theoretical result, and the derived PAS confirms the angular dispersion in the HSR channel. The angular dispersion is statistically characterized by the distance-based RMS AS model, and the statistical RMS AS results are compared in various HSR scenarios. It is also shown that when the antenna spacing is around 0.5 wavelength, almost all spatial correlation values are higher than 0.8 in the viaduct and cutting environments, however up to 45% of the values are lower than 0.8 in the station environment. Additionally, the proposed RMS AS-dependent spatial correlation model is able to efficiently describe the relationship between the angular dispersion and the spatial correlation. These results will provide useful information for channel modeling and performance evaluation in HSR multi-antenna communication systems.

References

[1] X. Cheng, L. Yang, and X. Shen, "D2D for intelligent transportation systems: A feasibility study," *IEEE Trans. Intell. Transp. Syst.*, vol. 16, no. 4, pp. 1784–1793, Aug. 2015.

[2] *White Paper for 5G High Mobility*. [Online]. Available: http://www.future-forum.org/ AQ:3

[3] *White Paper on 5G Vision and Requirements*. [Online]. Available: http://www.imt-2020.cn/

[4] T. L. Marzetta, "Noncooperative cellular wireless with unlimited numbers of base station antennas," *IEEE Trans. Wireless Commun.*, vol. 9, no. 11, pp. 3590–3600, Nov. 2010.

[5] T. Zhou, C. Tao, L. Liu, J. Qiu, and R. Sun, "High-speed railway channel measurements and characterizations: A review," *J. Modern Transp.*, vol. 20, no. 4, pp. 199–205, Dec. 2012.

[6] B. Ai *et al.*, "Radio wave propagation scene partitioning for high-speed rails," *Int. J. Antennas Propag.*, vol. 2012, pp. 815232-1–815232-7, Dec. 2012. AQ:4

[7] B. Ai *et al.*, "Challenges toward wireless communications for high-speed railway," *IEEE Trans. Intell. Transp. Syst.*, vol. 15, no. 5, pp. 2143–2158, Oct. 2014.

[8] C.-X. Wang, A. Ghazal, B. Ai, Y. Liu, and P. Fan, "Channel measurements and models for high-speed train communication systems: A survey," *IEEE Commun. Surveys Tut.*, vol. 18, no. 2, pp. 974–987, 2nd Quart., 2016.

[9] R. He, B. Ai, Z. Zhong, A. F. Molisch, R. Chen, and Y. Yang, "A measurement-based stochastic model for high-speed railway channels," *IEEE Trans. Intell. Transp. Syst.*, vol. 16, no. 3, pp. 1120–1135, Jul. 2014.

[10] K. Guan *et al.*, "Excess propagation loss modeling of semiclosed obstacles for intelligent transportation system," *IEEE Trans. Intell. Transp. Syst.*, vol. 17, no. 8, pp. 2171–2181, Aug. 2016.

[11] L. Liu *et al.*, "Position-based modeling for wireless channel on high-speed railway under a viaduct at 2.35 GHz," *IEEE J. Sel. Areas Commun.*, vol. 30, no. 4, pp. 834–845, May 2012.

[12] MEDAV. (2008). *RUSK Measurement Campaigns Overview*. [Online]. Available: http://www.medav.de/

[13] P. Kyösti *et al.*, "WINNER II channel models part II radio channel measurement and analysis results," 2007. AQ:5

[14] R. Parviainen, P. Kyösti, and Y. Hsieh, "Results of high speed train channel measurements," Eur. Cooperat. Field Sci. Tech. Res., Tech. Rep., 2008. AQ:6

[15] Q. Wang, C. Xu, M. Zhao, and D. Yu, "Results and analysis for a novel 2×2 channel measurement applied in LTE-R at 2.6 GHz," in *Proc. IEEE WCNC*, Istanbul, Turkey, Apr. 2014, pp. 177–181.

[16] B. Chen and Z. Zhong, "Geometry-based stochastic modeling for MIMO channel in high-speed mobile scenario," *Int. J. Antennas Propag.*, vol. 2012, pp. 184682-1–184682-6, Sep. 2012.

[17] T. Zhou, C. Tao, L. Liu, and Z. Tan, "A semiempirical MIMO channel model in obstructed viaduct scenarios on high-speed railway," *Int. J. Antennas Propag.*, vol. 2014, pp. 287159-1–287159-10, Sep. 2014.

[18] A. Ghazal, C.-X. Wang, B. Ai, D. Yuan, and H. Haas, "A nonstationary wideband MIMO channel model for high-mobility intelligent transportation systems," *IEEE Trans. Intell. Transp. Syst.*, vol. 16, no. 2, pp. 885–897, Apr. 2015.

[19] L. Tian, X. F. Yin, X. Zhou, and Q. Zuo, "Spatial cross-correlation modeling for propagation channels in indoor distributed antenna systems," *EURASIP J. Wireless Commun. Netw.*, vol. 2013, pp. 183-1–183-11, 2013.

[20] T. Zhou, C. Tao, S. Salous, Z. Tan, L. Liu, and L. Tian, "Graph-based stochastic model for high-speed railway cutting scenarios," *IET Microw., Antennas Propag.*, vol. 9, no. 15, pp. 1691–1697, Dec. 2015.

[21] T. Zhou, C. Tao, S. Salous, L. Liu, and Z. Tan, "Channel sounding for high-speed railway communication systems," *IEEE Commun. Mag.*, vol. 53, no. 10, pp. 70–77, Oct. 2015.

[22] B. Chen, Z. Zhong, B. Ai, and D. G. Michelson, "Moving virtual array measurement scheme in high-speed railway," *IEEE Antennas Wireless Propag. Lett.*, vol. 15, pp. 706–709, Mar. 2016.

[23] W. Wang, T. Jost, and A. Dammann, "Estimation and modelling of NLoS time-variant multipath for localization channel model in mobile radios," in *Proc. IEEE GLOBECOM*, Miami, FL, USA, Dec. 2010, pp. 1–6.

[24] E. G. Larsson, O. Edfors, F. Tufvesson, and T. L. Marzetta, "Massive MIMO for next generation wireless systems," *IEEE Commun. Mag.*, vol. 52, no. 2, pp. 186–195, Feb. 2014.

[25] X. Cai, X. F. Yin, and A. P. Yuste, "Direction-of-arrival estimation using single antenna in high-speed-train environments," in *Proc. 10th EuCAP*, Davos, Switzerland, 2016, pp. 1–4.

[26] S. Salous, *Radio Propagation Measurement and Channel Modelling*. West Sussex, U.K.: Wiley, 2013.

[27] O. Renaudin, V.-M. Kolmonen, P. Vainikainen, and C. Oestges, "Non-stationary narrowband MIMO inter-vehicle channel characterization in the 5-GHz band," *IEEE Trans. Veh. Technol.*, vol. 59, no. 4, pp. 2007–2015, May 2010.

[28] D. W. Matolak and R. Sun, "Air–ground channel characterization for unmanned aircraft systems—Part I: Methods, measurements, and models for over-water settings," *IEEE Trans. Veh. Technol.*, vol. 66, no. 1, pp. 26–44, Jan. 2017.

[29] A. Goldsmith, *Wireless Communications*, Cambridge, U.K.: Cambridge Univ. Press, 2005.

[30] M. D. Zoltowski and K. T. Wong, "Closed-form eigenstructure-based direction finding using arbitrary but identical subarrays on a sparse uniform Cartesian array grid," *IEEE Trans. Signal Process.*, vol. 48, no. 8, pp. 2205–2210, Aug. 2000.

[31] X. Cheng, C.-X. Wang, D. I. Laurenson, S. Salous, and A. V. Vasilakos, "An adaptive geometry-based stochastic model for non-isotropic MIMO mobile-to-mobile channels," *IEEE Trans. Wireless Commun.*, vol. 8, no. 9, pp. 4824–4835, Sep. 2009.

[32] X. Cheng, C.-X. Wang, B. Ai, and H. Aggoune, "Envelope level crossing rate and average fade duration of nonisotropic vehicle-to-vehicle ricean fading channels," *IEEE Trans. Intell. Transp. Syst.*, vol. 15, no. 1, pp. 62–72, Feb. 2014.

[33] X. Cheng, Q. Yao, M. Wen, C.-X. Wang, L.-Y. Song, and B.-L. Jiao, "Wideband channel modeling and intercarrier interference cancellation for vehicle-to-vehicle communication systems," *IEEE J. Sel. Areas Commun.*, vol. 31, no. 9, pp. 434–448, Sep. 2013.

[34] A. Abdi and M. Kaveh, "A space-time correlation model for multielement antenna systems in mobile fading channels," *IEEE J. Sel. Areas Commun.*, vol. 20, no. 3, pp. 550–560, Apr. 2002.

[35] X. Yin, X. Cai, X. Cheng, J. Chen, and M. Tian, "Empirical geometry-based random-cluster model for high-speed-train channels in UMTS networks," *IEEE Trans. Intell. Transp. Syst.*, vol. 16, no. 5, pp. 2850–2861, Oct. 2015.

[36] T. Zhou, C. Tao, L. Liu, and Z. Tan, "Ricean K-factor measurements and analysis for wideband high-speed railway channels at 2.35 GHz," *Radioengineering*, vol. 23, no. 2, pp. 578–585, Jun. 2014.

[37] *Sencity Rail Antenna: 1399.17.0039 HUBER+SUHNER Data Sheet, HUBER+SUHNERAG RF Industrial*, 2010. AQ:7

[38] T. Zhou, C. Tao, S. Salous, L. Liu, and Z. H. Tan, "Implementation of an LTE-based channel measurement method for high-speed railway scenarios," *IEEE Trans. Instrum. Meas.*, vol. 65, no. 1, pp. 25–36, Jan. 2016.

[39] R. He, Z. Zhong, B. Ai, J. Ding, Y. Yang, and A. F. Molisch, "Short-term fading behavior in high-speed railway cutting scenario: Measurements, analysis, and statistical models," *IEEE Trans. Antennas Propag.*, vol. 61, no. 4, pp. 2209–2222, Apr. 2013.

[40] K. Guan, Z. Zhong, B. Ai, and T. Kürner, "Propagation measurements and analysis for train stations of high-speed railway at 930 MHz," *IEEE Trans. Veh. Technol.*, vol. 63, no. 8, pp. 3499–3516, Oct. 2014.

[41] R. He, Z. Zhong, B. Ai, G. Wang, J. Ding, and A. F. Molisch, "Measurements and analysis of propagation channels in high-speed railway viaducts," *IEEE Trans. Wireless Commun.*, vol. 12, no. 2, pp. 794–805, Feb. 2013.

[42] M. Haardt and J. A. Nossek, "Unitary ESPRIT: How to obtain increased estimation accuracy with a reduced computational burden," *IEEE Trans. Signal Process.*, vol. 43, no. 5, pp. 1232–1242, May 1995.

[43] T. Zhou, C. Tao, L. Liu, and Z. H. Tan, "A study on a LTE-based channel sounding scheme for high-speed railway scenarios," in *Proc. IEEE 78th VTC-Fall*, Las Vegas, NV, USA, Sep. 2013, pp. 1–5.

[44] M. D. Zoltowski, M. Haardt, and C. P. Mathews, "Closed-form 2-D angle estimation with rectangular arrays in element space or beamspace via unitary ESPRIT," *IEEE Trans. Signal Process.*, vol. 44, no. 2, pp. 316–328, Feb. 1996.

[45] *Generation Partnership Project; Technical Specification Group Radio Access Network; Evolved Universal Terrestrial Radio Access (E-UTRA); Base Station (BS) Radio Transmission and Reception (Release 9)*, 3GPP, document TS 36.104 V9.3.0 3rd, 2010. AQ:8

[46] P. L. Kafle, A. Intarapanich, A. B. Sesay, J. Mcrory, and R. J. Davies, "Spatial correlation and capacity measurements for wideband MIMO channels in indoor office environment," *IEEE Trans. Wireless Commun.*, vol. 7, no. 5, pp. 1560–1571, May 2008.

[47] C. Oestges, D. Vanhoenacker-Janvier, and B. Clerckx, "Wide-band SIMO 1×2 measurements and characterization of outdoor wireless channels at 1.9 GHz," *IEEE Trans. Veh. Technol.*, vol. 53, no. 4, pp. 1190–1202, Jul. 2004.

Tao Zhou (M'16) received the B.E. degree from Changchun University of Science and Technology, Changchun, China, in 2009 and the Ph.D. degree from Beijing Jiaotong University, Beijing, China, in 2016.

From 2014 to 2015, he was a visiting Ph.D. Student with the Centre for Communication Systems, School of Engineering and Computing Sciences, Durham University, U.K. Since 2016, he has been an Associate Professor with Institute of Broadband Wireless Mobile Communications, School of Electronics and Information Engineering, Beijing Jiaotong University. His research interests include propagation channel characterization, channel sounding, and modeling for high-speed railway communication systems.

Cheng Tao (M'95) received the M.S. degree in telecommunication and electronic system from Xidian University, Xian, China, in 1989 and the Ph.D. degree in telecommunication and electronic system from Southeast University, Nanjing, China, in 1992.

He was a Post-Doctoral Fellow with the School of Electronics and Information Engineering, Beijing Jiaotong University (BJTU), Beijing, China, from 1993 to 1995. From 1995 to 2006, he was with the Air Force Missile College and the Air Force Commander College. In 2006, he joined as an Academic Faculty Member with BJTU, where he is currently a Full Professor and the Director of the Institute of Broadband Wireless Mobile Communications. He has authored over 50 papers and holds 20 patents. His current research interests include mobile communications, multiuser signal detection, radio channel measurement and modeling, and signal processing for communications.

Sana Salous (SM'95) received the B.E.E. degree from American University of Beirut, Beirut, Lebanon, in 1978, and the M.Sc. and Ph.D. degrees from Birmingham University, Birmingham, U.K., in 1979 and 1984, respectively. She was an Assistant Professor with Yarmouk University, Irbid, Jordan, for four years. She was a Research Fellow with Liverpool University, Liverpool, U.K., for one year. She held a Lectureship with University of Manchester Institute of Science and Technology, Manchester, U.K., in 1989, where she was subsequently a Senior Lecturer and then a Reader. Since 2003, she has been the Chair in communications engineering with Durham University, Durham, U.K., where she is currently the Director of the Centre for Communication Systems. Her research interests include radio channel characterization in various frequency bands ranging from skywave in the HF band to millimeter bands at 60 GHz, the design of radar waveforms, novel radio channel sounders, and radar systems for radio imaging.

Dr. Salous is a fellow of the Institution of Engineering and Technology. She is the Chair of the Commission C on Radio Communication and Signal Processing Systems of the International Union of Radio Science. She is an Associate Editor of *Radio Science* journal.

Liu Liu (M'12) received the B.E. and Ph.D. degrees from Beijing Jiaotong University (BJTU), Beijing, China, in 2004 and 2010, respectively.

He was a Post-Ph.D. Researcher with the School of Electronics and Information Engineering, Institute of Broadband Wireless Mobile Communications, BJTU, from 2010 to 2012, where he has been an Associate Professor Since 2012. His research interests include channel measurement and modeling for different propagation environments and signal processing of wireless communication in time-varying channel.

AUTHOR QUERIES

AUTHOR PLEASE ANSWER ALL QUERIES

PLEASE NOTE: We cannot accept new source files as corrections for your paper. If possible, please annotate the PDF proof we have sent you with your corrections and upload it via the Author Gateway. Alternatively, you may send us your corrections in list format. You may also upload revised graphics via the Author Gateway.

AQ:1 = Please confirm whether the corresponding authors information is correct as set.
AQ:2 = Please note that there were discrepancies between the accepted pdf [Measurements and Analysis of Angular Characteristics and Spatial Correlation for High-Speed Railway Channels_revised1_print.pdf] and the [Measurements and Analysis of Angular Characteristics and Spatial Correlation for High-Speed Railway Channels.tex] in the inline reference number and reference count. We have followed [Measurements and Analysis of Angular Characteristics and Spatial Correlation for High-Speed Railway Channels.tex].
AQ:3 = Please provide the accessed date for refs. [2] and [3].
AQ:4 = Please confirm the volume no. for refs. [6], [16], [17], and [19].
AQ:5 = Please confirm the author names, article title, and year for ref. [8]. Also provide the journal title, volume no., issue no., page range, and month.
AQ:6 = Please provide the organization, location, and report no. for ref. [14].
AQ:7 = Please confirm the title and year for refs. [37]. Also provide the organization name and organization location.
AQ:8 = Please confirm the title, document no., and year for ref. [45].